Summer 2020

cis-Resveratrol Upregulates Tyrosyl-tRNA Synthetase and Inhibits the Proliferation of Select Breast Cancer Cell Lines

Marion Cone Hope III

cis-Resveratrol Upregulates Tyrosyl-tRNA Synthetase and Inhibits the Proliferation of Select Breast Cancer Cell Lines

by

Marion Cone Hope III

Bachelor of Science
University of South Carolina, 2018

Submitted in Partial Fulfillment of the Requirements

For the Degree of Master of Science in

Biomedical Engineering

College of Engineering and Computing

University of South Carolina

2020

Accepted by:

Sajish Mathew, Director of Thesis

Özgur Şahin, Reader

Michael Gower, Reader

Cheryl L. Addy, Vice Provost and Dean of the Graduate School

Dedication

I would like to dedicate this work to my late grandfather Grover Jerry Hutson, affectionately known to his grandchildren as 'Grand'. He fought bravely with cholangiocarcinoma for 6 months until his death on February 14th, 2020. Grand was a self-proclaimed jokester and would enjoy long winded conversations with just about anyone. He worked as a trucker and my brother and I got to enjoy many vacations growing up where we joined him and my grandmother for a trip to wherever he was scheduled to deliver goods. If there were three things Grand loved the most, they would be his wife, daughters, and grandchildren. He never ceased talking about any of us and was so proud of all our accomplishments. In fact, all the nurses knew our names without us telling them because of his pride in who we were. We all loved him so much and are thankful for each moment we got to spend with him.

Acknowledgements

To my family for their continual support and constant encouragement over the past two years. Thank you for being there for me on days where I was tired and frustrated because I know there were many. I would like to thank my friend and mentor Megha Jhanji for teaching me everything I know when it comes to working in a lab, being a great listener, pushing me to do my best and for always being willing to help. To Dr. CNR for his friendly demeanor and our lighthearted conversations. To Dr. Vitali Sikirzhytski thank you for your time in developing the script and explanations of it. To Dr. Şhain for serving on my graduate committee and his lab for providing me with their cell stocks and help in various experiments. To Dr. Gower, thank you for taking time out of your busy schedule to serve on my committee. And finally, to my graduate advisor Dr. Sajish, thank you for allowing me to conduct research in your lab. I appreciate you taking a chance on me and helping me to become a better scientist and person.

Abstract

Breast cancer is one of the most commonly occurring cancers in women. 70% of breast cancer patients express ERα and are treated with tamoxifen (Tam), a drug that is used to directly target ERα. However, 20-30% of cancer patients develop a resistance to Tam. This resistance leads to a worse prognosis and other treatments such as DNA damaging drugs or radiation to eliminate these cells. Resveratrol (RSV) is a polyphenolic- compound found in plants such as grapes and hellebore and is known to evoke anti-cancer effects. While natural resveratrol exists as a mixture of both *cis*- and *trans*- isomers, so far, the isomer specific anti-cancer effects of RSV and their mechanisms of action of growth inhibitory effects are not well understood. Most recent studies have demonstrated that eukaryotic tyrosyl-tRNA synthetase (TyrRS)- an essential component of the protein synthesis machinery is a direct target of *cis*-RSV. While there are no apparent differences in the cellular levels of TyrRS in the WT T47D cells, treatment with *cis*-RSV resulted in a significant upregulation of TyrRS in the Tam resistant (TamR) T47D cells. Consistent with the inhibitory effect of *cis*-RSV on the L-tyrosine activation for protein synthesis by TyrRS, treatment with *cis*-RSV resulted in a greater growth inhibition in TamR T47D cells. Further, cellular signaling pathway analysis demonstrated that treatment with *cis*-RSV also resulted in a pronounced inhibitory effect on mammalian target of rapamycin complex 1 (mTORC1) signaling that drives protein synthesis in the TamR T47D cells. Therefore, *cis*-

RSV-mediated inhibition of mTOR signaling and TyrRS function in translation would in part be responsible for the growth inhibitory effects of *cis*-RSV. However, unlike *cis*-RSV, *trans*-RSV evoked growth inhibitory effects in both WT and TamR T47D. Although *trans*-RSV downregulated TyrRS in WT T47D, it did not affect TyrRS levels in TamR T47D. Therefore, utilizing a combination of growth inhibition assays, immunofluorescent imaging and western blot analysis primarily within WT and TamR T47D cells, this study implies that the anti-cancer effect of *cis*-RSV correlates with the cellular level of TyrRS whereas the anti-cancer effects of *trans*-RSV is independent of cellular level of TyrRS.

Table of Contents

List of Tables

List of Figures

Chapter 1

Introduction

1.1 Tamoxifen Resistance in Breast Cancer

260,000 new cases of breast cancer occurred in 2018 and of those 260,000 cases, 70% of these cancers express estrogen receptor (ERα)[1]. Tamoxifen (Tam) is a drug used to target ERα expressing cancer cells; furthermore, out of 70% of patients who are diagnosed with ERα expressing breast cancer, 20-30% of these patients develop resistance to hormonal therapy such as Tam (TamR)[2]. It is imperative to discover therapies that eliminate or sensitize resistant cancer cells, preferably, without causing carcinogenic events such as DNA damage in healthy cells to increase the effectiveness of widely used anti-cancer drugs.

1.2 Tamoxifen

Tam, one of the bestselling hormonal cancer compounds in the world, has been in extensive use since the 1980s to combat breast cancer and is a prodrug that can be administered orally to breast cancer patients via Tam citrate pills. In the liver, Tam is transformed by Cytochrome P450 enzymes into its active state of 4-Hydroxytamoxifen, which is a competitive antagonist of estrogen in binding to ERα[3]. Despite the extensive use and popularity of Tam, its molecular mechanism of action is not completely understood. Tam is classified as a selective ER modulator (SERM) because in addition to

anti-estrogenic properties displayed in the breast tissue via growth inhibition of breast cancer, Tam also exhibits estrogenic properties such as the proliferation of endometrial cells and promotion of bone density[4]. Moreover, the emergence of tumors resistant against Tam necessitates elucidation of the mechanism of the dual effects of Tam in combating Tam resistant breast cancer cells**.**

1.3 DNA Damage Signaling and Repair

DNA damage comes in forms ranging from lesions on the DNA, double-strand breaks (DSB) and single-strand breaks (SSB). Mechanisms to detect DNA damage and repair DNA were developed to prevent the accumulation of mutations and successful delivery of genetic information to the next generation[5].

Common DNA Repair mechanisms are base excision repair (BER), single-strand break repair (SSBR) and homologous recombination (HR). These repair mechanisms receive signals from either protein kinase ataxia-telangiectasia mutated (ATM) or ataxia-telangiectasia and Rad3 related (ATR) mediated DNA damage signaling[5]. BER is mediated through oxidative damage caused by lesions created by reactive oxygen species, which are then recognized and removed by damage specific glycosylases[6]. After removal of the damaged nucleotide, polymerase and ligase proteins are recruited to finish the repairs from the SSB that occurs from BER. Poly-ADP-ribose polymerase 1 (PARP1) is a major modulator that detects and binds to SSB that activates PARP1 resulting in the formation of poly-ADP-ribose (PAR) chains that recruit DNA repair factors to the site of DNA damage. Specifically, PARP1 activation leads to the recruitment of X-ray repair cross-

complementing protein 1 (XRCC1), an important scaffolding protein for proteins such as DNA ligase 3 which stimulate the repair process[7].

Double strand breaks (DSB) are signaled by the phosphorylation of histone H2A.X at Ser139 by ATM. Phosphorylation of H2A.X can build foci to recruit other proteins such as p53 and breast cancer associated gene 1 (BRCA1) to break and repair the damage[8]. HR is one method for repairing DSB signaled by phosphorylation of H2A.X that relies on the sister-chromatid sequences as a template for repair; therefore, HR can only occur in S or G_2 phases of the cell cycle. ssDNA loaded with Rad51 initiates HR leading to synapsis where Rad51 joins the homologous duplex DNA template with the invading DNA substrate. After the synapsis, the 3' end of the invading DNA acts as a primer for synthesis resulting in Rad51 dissociation from the newly formed double-strand DNA[9].

DNA damage mechanisms are frequently mutated/dysregulated in cancer cells. Dysregulated DNA damage response pathways (DDR) pathways trigger increased genomic instability and the accumulation of mutations that ultimately result in tumorigenesis. Consistently, cells that are particularly susceptible to tumorigenesis have defects in genes or protein mutations such as p53, ATM, or the BRCA family. In fact, in cells with mutant DNA damage proteins, the threshold for endogenous DNA breaks is higher in pre-cancerous cells[10]. Therefore, an efficient DNA repair machinery is part of the endogenous anti-cancer mechanisms and DDR is considered an anti-cancer barrier in early human tumorigenesis.

1.4 Autophagy in Breast Cancer

Autophagy is a catabolic process used by cells to prevent the accumulation of toxic substances such as excess proteins, pathogens, and improperly functioning organelles through the formation of an autophagosome. The autophagosome is formed to capture and degrade the aforementioned toxic substances by joining with lysosomes[11]. Autophagy, in conjunction with the ubiquitin-proteasome degradation pathway, are the central regulators in the maintenance of protein and organelle quality as well as the prevention of protein aggregation[12].

In the context of cancer, it has been observed that autophagy promotes tumor cell maintenance and survival in response to metabolic stress[13]. Metabolic stress-induced in cancer cells due to reliance on glycolysis for energy and rapid proliferation induces autophagy, which can generate more energy for the cell[11,14]. Furthermore, unregulated autophagy typically leads to apoptosis but does not under conditions in which apoptotic proteins such as Bcl-2 and BAX are mutated or downregulated[15].

Although the mechanism is not completely understood, autophagy activation during DNA damage can trigger apoptosis[16]. Consistently, some studies have reported cancer cell death that has resulted from the consumption of the cell through unregulated autophagy. Typically, cell death characterized by unregulated autophagy is characterized by the absence of chromatin condensation and an excessive number of autophagosomes in the cell. Many instances of autophagic death include a mutant version of the *BECN1* gene that codes for Beclin1 overcoming inhibition by Bcl-2[17]. Other mechanisms within autophagic cancer cell death include accumulation of p62, leading to activation of NF-κB

and retention of damaged organelles such as the mitochondria, which can produce reactive oxygen species[18]. Thus, under the right circumstances, the autophagy pathway can be targeted for therapeutic purposes.

1.5 Resveratrol: Mechanism of Action of Anti-Cancer Effects.

Resveratrol, 3,4',5-trihydroxystilbene, (RSV) is a phytoalexin and polyphenol that is produced in plants such as grapes and hellebore. Originally, RSV was hypothesized to be responsible for the cardioprotective effect of red wine but also has proposed anti-cancer and lifespan-extending effects[19,20]. In the original paper describing the anti-cancer effect of the *trans*- isomer of RSV the study found that *trans*-RSV was able to inhibit events that were associated with tumor promotion, progression, and initiation. Events related to each of these processes were the ability of *trans*-RSV to inhibit tumor initiation by preventing free-radical formation, inducing granulocyte expression indicative of nonproliferative phenotype to prevent tumor progression and inhibition of cyclooxygenase 1 for the prevention of tumor initiation[21]. Intriguingly, the anti-cancer effect of *trans*-RSV does not evoke a linear dose response *in-vivo*: lower doses of *trans*-RSV have better anti-cancer effects *in-vivo* compared to its higher concentrations, which result in negative effects such as weight gain[22].

1.5.1 trans-RSV is a direct activator of SIRT1

Early studies showed that *trans*-RSV is a direct activator of silent information regulation factor 1 (SIRT1). *trans*-RSV decreases the Michaelis constant of SIRT1 and promotes cell survival through SIRT1 dependent deacetylation (inactivation) of p53, to

extend the lifespan of *saccharomyces cerevisiae*[19]. Despite inhibiting p53 activation, SIRT1 is capable of evoking anti-cancer effects. Interestingly, the mRNA and protein expression levels of SIRT1 are linked to the expression of BRCA1, especially in BRCA1 mutated cells that exhibited lower levels of SIRT1. This finding led to experiments proposing that overexpression of SIRT1 would prevent tumor formation and consistently, overexpression of SIRT1 was able to inhibit BRCA1 mutated breast cancer growth. Based on the information that *trans*-RSV is an agonist of SIRT1, both *in-vitro* experiments with soft agar colonies and *in-vivo* experiments with nude mice were performed to test if *trans*-RSV activation of SIRT1 influenced cell growth. These studies displayed that *trans*-RSV treatment reduced the ability of BRCA1 mutant cells to form soft agar colonies *in-vitro* and delayed tumor formation and growth in nude mice leading to the assumption that SIRT1 activators such as *trans*-RSV may have therapeutic potential in BRCA1 mutant breast cancers[23].

Conversely, SIRT1 is also known to be involved with metastasis and proliferation of cancer cells through the activation of epithelial-mesenchymal transition (EMT). For example, deacetylation of Beclin-1 via SIRT1 induced autophagy, causing the degradation of E-cadherin, which is a major inhibitor of EMT. The degradation of E-cadherin increases cell migration and invasion in melanoma cells[24]. Another example of SIRT1 promoting cancer growth and metastasis is through the activation of the phosphoinositide 3-kinases/protein kinase B (PI3K/AKT) pathway[25,26]. As expected, overexpression of SIRT1 promoted cell proliferation both *in-vitro* and *in-vivo,* and conversely, knockdown of SIRT1 inhibited cell proliferation. Therefore, activation of SIRT1 results in either anti-cancer or

cancer-promoting effects depending on the cell type. These observations suggest that *trans*-RSV would also demonstrate similar anti-cancer or cancer-promoting effects depending on the cell type as *trans*-RSV is a direct activator of SIRT1[26].

1.5.2 Estrogenic and Anti-Estrogenic Effects of trans-RSV

trans-RSV has a similar structure to the physiological estrogen, 17β-estradiol (E2), and synthetic estrogen, diethylstilbestrol (DES). This similarity prompted research on the ability of *trans*-RSV to bind to ERα and if the binding of *trans*-RSV to ERα promotes estrogenic effects[27]. Competition binding studies performed with extracts of MCF-7 cells showed that *trans*-RSV was able to inhibit the binding of other estrogens at a concentration of 10 μM, which is a similar concentration to which *trans*-RSV exhibits its biological functions[21]. Further tests were performed determining the ability of *trans*-RSV to act as a super agonist through greater activation of estrogen response elements (ERE) than either E2 or DES. In addition to MCF-7, *trans*-RSV was tested in BG-1 ovarian carcinoma cells, which determined that *trans*-RSV dependent transcriptional activation was less than that of E2, providing evidence that *trans*-RSV may behave differently depending on tissue type. Finally, the study determined that *trans*-RSV promotes similar cell growth to E2 in T47D at a concentration of 10 μM, adding further evidence of the estrogenic effects of *trans*-RSV in breast cancer cells[27]. In confirmation of the super agonism claim not being limited to transiently transfected genes, MCF-7 with integrated ERE were utilized and again, *trans*-RSV acted as a super agonist[28]. E2 and *trans*-RSV have shown to differentially recruit coactivators such as steroid coactivators, SRC1, SRC2 and SRC3 when bound to ERα. Upon *trans*-RSV treatment, it was determined that full

association of ERα and SRC2 had been achieved but the interactions with SRC1 and SRC3 had been reduced and ERα was suspected of adopting a new conformation in the presence of *trans*-RSV and was shown to bind with two separate conformations. One conformation displayed the phenol mimicking the A ring of E2 and the second conformation has the resorcinol mimicking the A ring of E2. By way of either of these conformations, it appears that *trans*-RSV and E2 promote an anti-inflammatory effect by inhibiting the prominent inflammatory protein interleukin-6[29].

Several follow up studies have enforced that *trans*-RSV has estrogenic properties, but other studies have contrasted these findings though the discovery of anti-estrogenic effects. For instance, in a follow-up study to the effect of *trans*-RSV in promoting ERE, no super agonist or additive effects were observed. Furthermore, when *trans*-RSV and E2 were both added to T47D, it was determined that *trans*-RSV was an antagonist of E2. Expression of the estrogen inducible protein, pS2 with E2 treatment did not cause a change in overall protein expression, but when treated with *trans*-RSV expression of pS2 concentrations were decreased. In the NMU rat model, *trans*-RSV had no effect on body weight, increased the tumor latency, reduced the number of tumors, and tumor cells displayed cellular apoptosis at the periphery of the tumor as compared to the center of the tumor for the control group at a concentration of 100 mg/kg but displayed no difference from the control group at a concentration of 10 mg/kg[30]. *trans*-RSV in the absence of ERE through transcriptional activation domain AF-1 deletion, C-terminal deletion or in the presence of an ERα negative cell line such as MDA-MB-231 maintains production of a stimulatory effect for luciferase and for cells without ERE because the

transcriptional activation domain AF-2 deletion increases induction of transforming growth factor α signifying that not all *trans*-RSV functions are dependent on ERα[28]. It could be ascertained that *trans*-RSV could belong to the class of SERMs such as Tam as its estrogenic and anti-estrogenic effects are tissue and case-specific. Seeing as *trans*-RSV has SERM qualities, this study aims to determine if *trans*-RSV has any similarities to Tam in promoting cell apoptosis and if *cis*- and *trans*-RSV action is independent of ERα.

1.5.3 trans-RSV is a direct inhibitor of phosphodiesterase (PDE)

Among the PDEs, PDE4 is a cAMP-selective hydrolase and was found to be inhibited by *trans*-RSV, resulting in the activation of AMP-activated protein kinase alpha (AMPKα)[31]. Molecular docking simulation and binding free energy reactions further confirmed that *trans*-RSV is a direct inhibitor of PDE4, specifically the PDE4D subunit[32].

Interestingly, *trans*-RSV was indicated to prohibit breast cancer growth and increase cyclic adenosine monophosphate (cAMP) levels both alone and with pretreatment of two phosphodiesterase inhibitors (PDEi), IBMX and rolipram. The combination of PDEi and *trans*-RSV induced growth inhibition and cAMP levels are greater than *trans*-RSV or PDEi alone. These results lead to the study concluding that *trans*-RSV did not directly inhibit PDE, but instead to *trans*-RSV dependent activation of adenylate cyclase[33]. Building upon the information that cAMP plays a role in the function of *trans*-RSV, another group investigated the original claims of PDE inhibition and if cAMP production was the cause of *trans*-RSV mediated AMPKα activation. HeLa and myotube cells were treated with resveratrol in the presence of an adenylate cyclase inhibitor,

which showed no increase in the phosphorylation of AMPKα. This result was used to support the necessity of cAMP signaling for the effect of *trans*-RSV[34].

1.6 PDE4D inhibition overcomes Tamoxifen Resistance.

Recent works from Dr. Özgur Şahin's group demonstrated that PDE4D inhibition is a potential mechanism to overcome Tam resistance in TamR cells. Whole transcriptome analysis of TamR MCF-7 and T47D cells and pathway enrichment analysis showed that cAMP-mediated signaling pathways are enriched in the TamR cells compared to the WT cells, which suggested a possible role of cAMP in the acquisition of Tam resistance. qRT-PCR analysis revealed that PDE4D was one of the most upregulated genes in the TamR cells that can be targeted with therapeutics. As hypothesized either inhibition of PDE4D using small molecules or knocking it down using siRNA, the TamR cells were sensitized to Tam. Consistently, Kaplan-Meier (K-M) plotting showed that PDE4D expression played a role in the prognostic patient outcome and increased PDE4D expression in patients who were treated with tamoxifen lead to a worse outcome[35].

Although *trans*-RSV is also known to inhibit PDE4D[31], it is not yet known if treatment with *trans*-RSV would overcome Tamoxifen resistance. Therefore, in this study, we hypothesize that trans-RSV sensitizes TamR cells via inhibition of PDE4D; however, it is unknown if PDE4D is a specific target of *trans*-RSV or if its effect on PDE4D inhibition is an off-target effect[36].

1.7 *cis*-RSV binds to tyrosyl-tRNA synthetase (TyrRS) to promote genetic stability through PARP1 and activate cAMP signaling pathways.

RSV exists as *cis*- and *trans*- isomers (*cis*-RSV and *trans*-RSV) and *trans*-RSV is known to activate p53 through the induction of DNA damage which triggers genomic instability- a hallmark of cancer and causing *trans*-RSV to promote cancer growth[37,38,39]. However, recent works demonstrated that tyrosyl-tRNA synthetase (TyrRS) is a novel target for *cis*-RSV that activates PARP1 and p53- major determinants of genomic stability that prevents carcinogenesis[40].

PARP1 and its closely related protein Poly-ADP-Ribose Polymerase 2 (PARP2) are integral to all DNA Damage response pathways[41]. When PARP protein is not present in the cell spontaneous tumor generation will occur[42]. And in cancers such as lymphoma, where mutation to DNA Damage response proteins drives tumor progression, the loss of PARP is lethal[43]. This is important, because classically PARP has been inhibited for cancer therapy, however a study from 2020 shows that treatment with the FDA approved PARP inhibitor, Olaparib, exacerbates bone metastasis in various mouse xenograft models[44]. These studies provide evidence that PARP activation is necessary in maintaining genomic stability and promoting inquiry into if PARP activation can have an anti-cancer effect.

Interestingly K-M plotting shows, when PARP1 activator, TyrRS, has higher mRNA expression in breast cancer patients there is a worse prognosis[45]. The results from the K-M can be explained through the function of TyrRS. TyrRS is a protein critical to protein translation with a primary physiological role in activating and charging L-tyrosine to

tRNA[46]. Meaning that increased TyrRS expression should lead to increased proliferation. Both *cis*- and *trans*-RSV and are competitive inhibitors of L-tyrosine and can inhibit the function of TyrRS in translation, however only the *cis*-RSV conformation can activate PARP1[40]. Based on this information we hypothesize that both *cis*- and *trans*-RSV will inhibit translation by preventing the physiological function of TyrRS.

Furthermore, the PARP1-dependent production of ADP-ribose (ADPR) is a potent inhibitor of PDEs[47]. Therefore, *cis*-RSV-mediated activation of PARP1 would result in the transient upregulation of cAMP levels. These observations also suggest that *cis*-RSV can have anti-cancer effects depending on the cell type. Therefore, despite acting through distinct molecular targets, we hypothesize that both *cis*- and *trans*-isomers of RSV would overcome tamoxifen resistance.

Chapter 2

Materials and Methods

2.1 Cell Lines and Culture Conditions

The ATCC breast cancer cell lines, SK-BR-3, JIMT1, BT-474 and HCC1954 were gifts from Dr. Igor Roninson, and WT MCF-7, TamR MCF-7, WT T47D and TamR T47D were gifts from Dr. Özgur Şahin. WT cell lines were bought from ATCC. All TamR cell lines were developed by Dr. Şahin's group per their previous protocol[48]. SK-BR-3 and BT-474 were cultured in DMEM (GE Lifesciences) with 1% (v/v) Penicillin/Streptomycin, 1% (v/v) L-glutamine and 10% fetal bovine serum (FBS). JIMT-1 and HCC1954 were cultured in RPMI 1640 (GE Lifesciences) with 1% (v/v) Penicillin/Streptomycin, 1% (v/v) L-glutamine and 10% FBS. WT and TamR MCF-7 and T47D cell lines were cultured in phenol red free DMEM (GE Lifesciences) with 1% (v/v) Penicillin/Streptomycin, 1% (v/v) non-essential amino acids, 0.1% (v/v) insulin from bovine pancreas (Sigma-Aldrich), and 10 % (v/v) heat-inactivated FBS. All cells were maintained in 37 °C at 5% CO_2 humidified atmosphere in an incubator. To ensure MCF-7 and T47D TamR cells remained resistant to Tam; 5 µM Tam was added to cells for 72 hr in two subsequent passages after every five passages of normal cell culture.

2.2 Passaging Cells

1X PBS was used to wash cells, and then 0.05 % Trypsin (SH3023601, Invitrogen) was used to disrupt the interaction of the cells with the surface of the 100 mm x 20 mm cell culture dish. Dish with 0.05 % Trypsin was placed in 37 °C incubator for 3-5 min. Cell culture media was added to dish and collected in a 15 mL centrifuge tube (Corning) and spun at 13,000 RPM for 3 min. The supernatant was removed from the cell pellet, and the cell pellet was washed with cell culture media. Hemacytometer was used to count cells before seeding into either 100 mm x 20 mm cell culture dish, 6 Well Plate, or 96 Well Plate.

2.3 Cell Viability Assays

Growth inhibition of cells treated with compounds such as *cis*- and *trans*-RSV was evaluated via Pro-Mega CellTiter-Glo Luminescent Cell Viability Assay as well as the MTT Assay. Dr. Sahin's lab performed the Pro-Mega CellTiter-Glo Luminescent Cell Viability Assay to determine the growth inhibition for WT and TamR MCF-7 and T47D cell lines. All WT and TamR MCF-7 were treated with 50 μM of *cis*- or *trans*-RSV alone and in combination with Tam (2.5 μM for WT and 7.5 μM for TamR) for 72 hr in a 96 well plate. All WT and TamR T47D were treated with 50 μM *cis*- or *trans*-RSV alone or in combination with 5 μM Tam for 72 hr in a 96 well plate. 100μL of CellTiter-Glo Luminescent assay was added to the wells, placed on an orbital shaker for 2 min and incubated at room temperature for 10 min. Finally, the luminesce of the sample was recorded. 3-(4,5-dimethylthiazol-2-yl)-2,5-diphenyltetrazolium bromide (MTT) assay was performed on

SK-BR-3, HCC1954, JIMT-1 and BT-474 cell lines. Cells were seeded in 96 well plates with a density of 1,500 cells/well for SK-BR-3, JIMT-1, BT-474 and 3,000 cells/well for HCC1954. Cells were given a minimum of 16 hr to grow before treatment. All cells were treated with 0, 10, 25, 50, 75 and 100 µM of *cis*- or *trans*-RSV and incubated for 72 hr. 10 µL of MTT was added in each well and incubated for 2 hr. Plates were removed from incubator and media was discarded. Next, 100 µL of DMSO was added to each well and mixed by pipetting. Finally, absorbance values at 570 nm were recorded.

2.4 Western Blot Analysis

Both WT and TamR T47D cells were seeded at 300,000 cells/well in a 6 well culture plate, grown for 40 hr and treated with either 50 µM *cis*- or *trans*-RSV alone or in combination with 5 µM Tam for 24 hr. Cells were washed with chilled 1X PBS (GE Healthcare) and collected with 1X SDS loading buffer. Next, cell lysates underwent sonication and quantification with BCA Quantification Kit (Thermo Fisher). Lysates of 9 µg were run on NuPAGE Bis-Tris Gels (Invitrogen) and transferred onto nitrocellulose membranes (iBlot Transfer Stack, Invitrogen) with an iBlot transfer system (Invitrogen). Blots were blocked with 5% (m/v) non-fat milk (NFM) in 1X TBST for 1 hr. Primary antibodies were diluted in 5% (m/v) in BCA in 1X TBST, placed on blots and left to incubate overnight at 4 °C. β-Actin (8H101D10, Cell Signaling Technology) and was used as the loading control. β-Actin was diluted 1:1000 in 5 % (m/v) BSA in 1X TBST. Blots were incubated with secondary Anti-mouse IgG, HRP-linked antibody and Anti-rabbit IgG, HRP-linked antibody (7076&7074, Cell Signaling Technology) diluted 1:10000 in 5 % (m/v) NFM in 1X TBST for 1 hr at room temperature. Immobilon ECL Ultra Western HRP Substrate

(Millipore) was used to develop signals from HRP-conjugated secondary antibodies. Western Blots were imaged with a Bio-Rad ChemiDoc MP Imaging system, were cropped with ImageLab, and quantified as 8-bit images in Fiji. Excel was used to store quantification data and normalize all proteins to the loading control, β-Actin. The primary antibodies used in DNA damage response analysis are listed as follows, phospho-Histone H2A.X Ser139 (20E3, Cell Signaling Technology), phospho-Histone H3 Ser10 (D2C8), Checkpoint Kinase 2 (CHK2) (2662, Cell Signaling Technology), phospho-CHK2 Thr68 (C13C1, Cell Signaling Technology), p53 (1C12, Cell Signaling Technology), phospho-p53 Ser15 (9284, Cell Signaling Technology) and Bim (C34C5, Cell Signaling Technology). Primary antibodies used in autophagy analysis include, AMPKα (2532, Cell Signaling Technology), phospho-AMPKα Thr172 (40H9, Cell Signaling Technology), Unc-51 like autophagy activating kinase (ULK1) (D8H5, Cell Signaling Technology), phospho-ULK1 Ser 757 (6888, Cell Signaling Technology), Beclin 1 (D40C5, Cell Signaling Technology) and microtubule-associated protein 1A/1B-light chain 3 (LC3A/B) (D3U4C, Cell Signaling Technology). Primary antibodies used in protein translation analysis include S6 Ribosomal Protein (S6) (5G10, Cell Signaling Technology), phospho-S6 Ser235/236 (2211, Cell Signaling Technology), phospho-S6 (Ser240/244) (2215, Cell Signaling Technology), 4E-BP-1 (53H11 , Cell Signaling Technology), phospho-4E-BP-1 Thr37/46 (236B4, Cell Signaling Technology), eukaryotic initiation factor 2 α (eIF2α) (9722, Cell Signaling Technology), and phospho-eIF2α Ser51 (9721, Cell Signaling Technology). Mammalian target of rapamycin (mTOR) (2972, Cell Signaling Technology) and phospho-mTOR Ser2448 (2971, Cell Signaling Technology) were also utilized in this study.

2.5 Immunoprecipitation Analysis

MCF-7 WT and TamR cells were seeded as mentioned in section 2.4. Both MCF-7 WT and TamR cells were treated with 50 µM of *cis*- and *trans*-RSV for 1 hr. Cells were washed twice with chilled 1X PBS and were processed with Cell Signaling Technology 1X Cell Lysis Buffer: 20 mM Tris-HCl (pH 7.5), 150 mM NaCl, 1 mM Na_2EDTA, 1 mM EGTA, 1% Triton, 2.5 mM sodium pyrophosphate, 1 mM beta-glycerophosphate, 1 mM Na_3VO_4, 1 µg/ml leupeptin. An additional 0.5 % (v/v) Triton X-100 was added to the cell lysis buffer to reach nuclear proteins as well as a Protease Inhibitor Cocktail Tablet (5892970001, Roche). Cells remained in lysis buffer for 10 min on ice and then were harvested and sonicated. Lysate was quantified with BCA Quantification Kit and appropriate amount of whole cell lysate was removed from sample for IP while remaining whole cell lysate was harvested for a western blot. Whole cell lysate for western was mixed with SDS loading dye and appropriate cell lysis buffer to load 5 µg-7 µg of protein. Lysis buffer used for IP was collected for a 50, 75, 100 or 150 µg pulldown. PARP1 IP was conducted by adding PARP1 (556494, BD Biosciences) 1:200 dilution to each sample which were incubated at 4 °C for 45 min. 50 µL of rProtien G Agarose Beads (15920-01, Novex Life Technologies) in 5 % (m/v) BSA in 1X TBST were added to each sample and were incubated for 30 min at 4 °C. Next, samples were washed 3 times with cell lysis buffer through centrifugation for 5 min at 1000 rpm. After the last centrifugation for 5 min at 1000 rpm cell lysis buffer was removed from the samples and 50 µL of 1X SDS loading buffer was added to each sample. Samples were boiled for 2 min at 95 °C and run on NuPAGE Bis-Tris Gels (Invitrogen) and transferred onto nitrocellulose membranes (iBlot Transfer Stack, Invitrogen) with an iBlot

transfer system (Invitrogen). Anti-PAN ADPr binding agent (Oligo-ADP-Ribose) (MABE1016, Milipore), TyrRS (NBP1-32551, Novus Biologicals), and PARP1 (556494, BD Biosciences). Immunoblots used the same blocking, secondary antibody and were developed as described in 2.4

2.6 Immunofluorescence

2.6.1 Cell Treatment and Staining

Coverslips were prepared by a 1 hr nitric acid treatment followed by washing with DI H_2O 15-20 times. Coverslips were then washed in absolute ethanol and stored in the cell culture hood where they would be utilized. Both MCF-7 and T47D WT and TamR cells were seeded on coverslips 300,000 cells/well for a minimum of 16 hr before treatment. Cells were treated with *cis*- or *trans*-RSV (50 mM) for 1 hr, washed with 1X PBS and then fixed with 2 % (v/v) PFA in 1X PBS for 15 min. Next, cells were washed three times with 1X PBS and permeabilized with 0.2 % (v/v) in 1X PBS for 5 min. After 3 more washes with 1X PBS coverslips were blocked with 3 % (m/v) BSA in 1X TBST for 30 min. Primary antibody TyrRS (NBP1-32551, Novus) was diluted 1:300 in 3 % (m/v) BSA in 1X TBST and 80 µL of antibody solution was added to the surface of a glass sheet wrapped in parafilm in a humidification chamber. Coverslips were placed cells side down on the antibody solution and incubated in 4 °C overnight. Coverslips were removed from 4 °C and washed three times with 1X PBS. Secondary antibody Anti-Rabbit Alexa Fluor 488 (Green) (Invitrogen) was diluted 1:1000 in 3% (m/v) BSA in 1X PBS. Coverslips were then incubated on 80 µL of secondary antibody solution in the humidification chamber for 1 hr at room

temperature. The coverslips were removed from the humidification chamber in the dark and washed 3 times for 10 min each in the dark. Finally, coverslips were mounted with Antifade Gold Mountant with 25 µL DAPI (Invitrogen). Coverslips were imagined using Carl Zeiss LSM700 Confocal Microscope 63X magnification.

2.6.2 Processing of Images for protein intensity and localization through Fiji

This section provides the information regarding the Java Script, Protein_Expression_and_Colocalization, used for the detection of TyrRS total protein expression and localization developed by Dr. Vitali Sirkirzhytski of the University of South Carolina College of Pharmacy Microscopy Core for the Center of Targeted Therapeutics. The script was developed for use in Fiji and automated functions of preexisting Fiji tools for high throughput analysis. Image regions were selected according to manually selected thresholds. Thresholds for each channel were carefully chosen to count all meaningful information from a fluctuating signal of the fluorescence signal and minimize noise and background contributions. To minimize a human factor, the final thresholds were set using levels independently determined by different investigators. The thresholds selected for this study are listed as follows, the threshold for nucleus = 400, for cytoplasm = 800, to count green channel = 1750, and to count blue channel = 400. **Figure 2.1** demonstrates localization of nuclei (DAPI, blue fluorescence stain specific for double-stranded DNA) and TyrRS Anti-Rabbit Alexa Fluor 488 (Green) stained protein. **Figure 2.1A** shows DAPI stained nuclei outlined by yellow contours defined by the threshold level (400) shown as a sick black line in **Figure 2.1B**. **Figure 2.1B** shows the intensity profile along the yellow line in **Figure 2.1A**. The selected threshold level ensures correct detection of all nuclei

pixels (above the black line) and exclusion of low-intensity background regions. The localization of TyrRS protein is shown in **Figure 2.1C**. The region outside of the nucleus was estimated using contrast-enhanced green fluorescence channel **Figure 2.1D**. Characteristic spatial distribution of green fluorescence marker (TyrRS) allows effective detection of cytoplasm using threshold below the intracellular background level for the green channel. Size filter (1000 pixels) was introduced to eliminate the potential contribution of very small objects that originated from cell debris, fragmented nuclei, and dirt particles. All described parameters were incorporated into Fiji macros (IJ1 Macro scripting language) for completely automatic processing of image sets. After installation through Fiji macros plugins, a new icon/button is added to the panel of standard Fiji tools. When clicked, the dialog window allows the processing of a single .tif image or all images within the selected folder. Areas and mean intensities for the described above objects and regions are automatically saved as .csv files.

Protein localization was determined using raw mean intensity measurements determined by the script. Mean intensity of the nucleus was determined through the raw nuclear intensity values, mean intensity of the cytoplasm was determined through the raw cytoplasm intensity values and the mean intensity for the whole cell was determined through the average of the raw nuclear and the raw cytoplasm intensity values. Results derived from the script were validated through manual selection of the nucleus and the total cell by using the Measure function in Fiji to determine the mean intensity of each cell. For figure creation, green channel was replaced with Red Hot LUT to accent difference in protein levels and colocalization.

2.7 Statistical Analysis

Student's t-test was used to determine statistical significance between treatments in growth inhibition assays. One-way ANOVA with post hoc Tukey-Kramer and student t-test was used to determine statistical significance for western blots and immunofluorescent imaging. Error bars are calculated as mean ± standard error of the mean in all experiments.

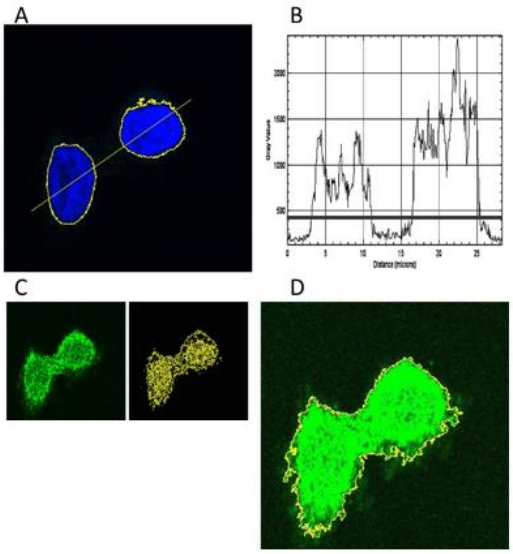

Figure 2.1. Calculations performed by Protein_Expression_and_Colocalization Script. Both WT and TamR MCF-7 and T47D cell lines were subjected to carefully selected manual thresholds for TyrRS and DAPI. Thresholds were selected to include all meaningful information from the fluctuating fluorescent signal to minimize noise. **(A)** Software capture of individual DAPI stains to outline the nucleus for analysis by a threshold level of 400. **(B)** Display of intensity profile along the yellow line in **(A)**. Peaks correspond to DAPI stain. **(C)** The localization of TyrRS is displayed as selected by the threshold. **(D)** Area for the cytoplasm was estimated using the contrast-enhanced green channel.

Chapter 3

Results

3.1 *cis*-Resveratrol Upregulates Tyrosyl-tRNA Synthetase and Inhibits the Proliferation of Select Breast Cancer Cell Lines.

Our previous work showed that treatment with low doses of natural RSV (<5-10 μM) induces the upregulation of the protein levels of TyrRS while facilitating its nuclear localization[40]. However, the isomer specific effect of RSV (*cis*-and *trans*-RSV) on the protein levels of TyrRS and its nuclear localization have not yet been explored. To test the isomer specific effect of RSV on TyrRS level, T47D breast cancer cells were treated with *cis*- and *trans*- RSV. After 1 hr of treatment with *cis*- and *trans*-RSV (50 μM), T47D were fixed and stained for immunofluorescent imaging using anti-TyrRS antibody. Quantification of the immunofluorescence for TyrRS showed that treatment with *trans*-RSV resulted in a significant decrease in the whole cell as well as both the nuclear and cytoplasmic levels of TyrRS, while treatment *cis*-RSV resulted in a slight decrease in the whole cell and the nuclear and cytoplasmic levels of TyrRS **(Fig. 3.1A and B and Fig 3.2)**. However, treatment with both *cis*- and *trans*-RSV in the TamR T47D cells lead to an increase in TyrRS protein level in the whole cell as well as the nucleus and cytoplasm. **(Fig 3.1A and B and Fig 3.2)** In addition to immunofluorescence, western blotting was used to

determine the change in TyrRS protein level after treatment with *cis*- or *trans*-RSV. Neither treatment with *cis*- or *trans*-RSV influenced total TyrRS protein level in the WT T47D cells, but in the TamR T47D *cis*-RSV increased the level of TyrRS present after 24 hr **(Fig 3.3)**. These results were interesting as not only were the total TyrRS levels increased, but there was a significantly large increase of TyrRS in the nucleus as well. Because upregulation of TyrRS is known to evoke PARP1-dependent cAMP signaling pathways and cAMP also overcomes tamoxifen resistance, we tested if treatment with cis-and trans-RSV would induce cytotoxic effects in T47D TamR cells[35,47]. Growth inhibition analysis after 72 hr of treatment with Tam, *cis*- or *trans*-RSV alone or in combination with Tam show that Tam in the WT, c*is*-RSV in combination with Tam in the WT and *cis*-RSV in the TamR context all promote similar levels of growth inhibition. When *cis*-RSV treatment in the WT is compared to treatment in the TamR there is an increase in growth inhibition in the TamR cells. Finally, the highest level of growth inhibition is exerted by the combination of *cis*- and Tam in the TamR T47D **(Fig 3.1C)**. When added to either WT or TamR T47D *trans*-RSV alone or in combination with Tam has the same level of growth inhibition **(Fig 3.1D)**. In addition to treatment at 50 μM, WT and TamR were treated in a dose-response manner permitting the study to specifically select 50 μM for the remainder of the treatments as the most obvious difference between *cis*-RSV treatments are located at that concentration **(Fig 3.4)**. The results from the immunofluorescent and growth inhibition assays imply that *trans*-RSV inhibit growth independent of TyrRS. However, it appears that treatment with *cis*-RSV, in a context such as TamR T47D, that there is a

correlation with the upregulation of TyrRS protein levels and growth inhibitory effects of *cis*-RSV.

To determine if the effects on growth inhibition and upregulation of TyrRS protein levels were specific to T47D, we tested the effect of cis- and trans-RSV in the MCF-7 cell line. Interestingly, there was no change in the growth inhibitory effect of *cis*-RSV between the WT and TamR MCF-7 **(Fig 3.5A)**. Although *trans*-RSV demonstrated significant growth inhibition in both MCF-7 WT and TamR cells the *trans*-RSV-mediated growth inhibition was unexpectedly lower in the TamR than the WT MCF-7 **(Fig 3.5B)**. A dose response assay confirmed this result **(Fig 3.6)**. Intriguingly, immunofluorescent analysis revealed that that treatment with both *cis*- and *trans*-RSV treatment lead to the decrease in the total level of TyrRS in the WT and TamR MCF-7 **(Fig 3.5C and D)** despite no significant difference in the total, nuclear or cytoplasmic protein expression of TyrRS between WT and TamR **(Fig 3.7A and B).** In addition to the total level of TyrRS being decreased, the nuclear and cytoplasmic levels were decreased in both cell types for both treatments and of great interest is the decrease in nuclear TyrRS protein level with *cis*-RSV treatment **(Fig 3.7C)**. These results provide further evidence that the cytotoxic ability of trans-RSV is independent of TyrRS protein levels and that the cytotoxic ability of *cis*-RSV is dependent of TyrRS protein level, specifically the level of TyrRS in the nucleus.

3.2 Growth Inhibition of *cis*- and *trans*-RSV on Various Breast Cancer Cell Lines

The difference, if any, in isomer specific growth inhibition of breast cancer cells of a wide range of subtypes by RSV has not been investigated. This set of experiments aimed

to determine the difference or lack thereof in growth inhibition between the two isomers and identify potential targets for *cis*-RSV treatment. Alternatively, both T47D and MCF-7 express high mRNA levels of ERα, progesterone receptor (PR) and low expression of human epidermal growth factor receptor 2 (HER2) and it is important to determine if the growth inhibition induced by *cis*- and *trans*-RSV is dependent on cell receptor expression. This especially pertains to ERα, as it has been reported that *trans*-RSV can bind to ERα inducing estrogen like effects[29]. Cells were treated with either *cis*- or *trans*-RSV to compare the difference in growth inhibition and determine which cells lines are most susceptible to treatment. Four different breast cancer cells of varying subtypes different than that of T47D and MCF-7 were chosen to analyze isomer and receptor specific growth inhibition. The selected breast cancer cell lines were HCC1954, JIMT-1, SK-BR-3 and BT-474. HCC1954, JIMT-1 and SK-BR-3 are all cells that express low amounts of mRNA for ERα and PR and have high expression of HER2. BT-474 expresses high amounts of mRNA for ERα, PR and HER2. (**Table 3.1** is provided in the appendix to reference receptor type of each cell line used in this study). Despite having similar receptor status, HCC1954, SK-BR-3 and JIMT-1, all responded to *cis*- and *trans-RSV* differently. Both *cis*- and *trans*-RSV induced growth inhibition in HCC1954 and was the only cell line where *cis*- induced higher inhibition than *trans*-RSV in **(Fig 3.8A)**. In JIMT-1 *trans*-RSV began to induce growth inhibition at 50 μM and *cis*-RSV at 100 μM **(Fig 3.8B)**, while SK-BR-3 provided mixed results with growth inhibition at 10, 50 and 100 μM for *trans*- and 100 μM for *cis*-RSV **(Fig 3.8C)**. Intriguingly, both *cis*- and *trans*-RSV evoked a growth-stimulating effect in BT-474, a cell line that has high expression of ERα, PR and HER2, until 100 μM **(Fig 3.8D)**. These data

indicate that the best candidates for growth inhibition by RSV are cells that overexpress ERα, PR and have a lesser expression of HER2, particularly for *trans*-RSV sharing similar levels of inhibition between MCF-7 and T47D or the particular case of the ERα negative, PR negative and HER2 positive HCC1954. It can also be suggested that cell receptor status is not the best indicator for the effectiveness of RSV as HCC1954 displayed the highest inhibition for *cis*-RSV and has the same receptor status as other cells where neither *cis*- or *trans*-RSV had an effect. All IC50 values from growth inhibition analysis are found in **Table 3.2**. As *cis*- has a higher inhibition than *trans*-RSV in HCC1954, it would be interesting to ascertain the TyrRS protein levels in this cell line. Ultimately, we decided to focus on the growth inhibitory mechanism using T47D WT and TamR cell lines.

3.3 Isomer specific Cell Signaling Analysis

3.3.1 Inhibition in protein translation signaling by cis- and trans-RSV

The main function of TyrRS is in protein translation, but when *cis*- or *trans*-RSV is bound to TyrRS its function in protein synthesis is inhibited, however our previous study used natural RSV as opposed to the specific isomers[40,46]. Considering this information, it was hypothesized that both isomers of RSV would inhibit protein translation signaling. WT and TamR T47D were treated with either Tam or *cis*- or *trans*-RSV alone and in combination with Tam and were processed for western blot. Inhibition of ribosomal translation signaling was observed in *cis*-RSV treatment for both the WT and TamR T47D context. Both showed a decrease in the phosphorylation of S6 Ribosomal Protein at the Ser235/236 and Ser240/244 sites. While treatment with *cis*-RSV did not change the

phosphorylation of 4E-BP-1 Thr37/46 in WT T47D there was a decrease in phosphorylation in TamR T47D **(Fig 3.9A)**. Inhibition of ribosomal translation signaling was also observed in *trans*-RSV for both WT and TamR T47D as seen by the decrease in phosphorylation of S6 Ribosomal Protein at the Ser235/236 and Ser240/244 sites **(Fig 3.9B)**. These results are expected as the inhibition in function of a tRNA synthetase such as TyrRS should lead to an inhibition of translation. It can be concluded from this data that both *cis*- and *trans*-RSV inhibit translation signaling in WT and TamR T47D.

mTOR complex 1 (mTORC1) signaling was investigated due to the decrease in phosphorylation of the downstream mTORC1 targets, 4E-BP-1 Thr37/46 and S6 Ser240/244 after treatment with *cis*-RSV. Western blotting after treatment with *cis*-RSV revealed that phosphorylation of the major mTORC1 determinant, mTOR Ser2448 was not changed in the WT T47D context, but was decreased in TamR T47D **(Fig 3.10)**[49]. This is consistent with the phosphorylation state of 4E-BP-1 Thr37/46 in both WT and TamR T47D the decrease in phosphorylation of S6 Ser240/244 in TamR T47D and provides evidence that a decrease in mTOR signaling is a determining factor in the unique effect observed by *cis*-RSV treatment in TamR T47D.

3.3.2 Induction of autophagy by trans-RSV in WT and by cis-RSV in TamR T47D

mTOR is a prominent inhibitor of autophagy and its inhibition is one of the first steps in the initiation of autophagy[50]. The previous section provided evidence for the inhibition of mTOR signaling so it was decided to study autophagy to illuminate if *cis*-RSV has a unique effect on this pathway. Induction of autophagy was studied in WT and TamR

T47D that were treated with either Tam or *cis* or *trans* -RSV alone and in combination with Tam was monitored through western blot analysis. In the *cis*-RSV treatment the relationship between treatment and autophagy was altered between the WT and TamR T47D. *cis*-RSV protein levels in the WT context did not provide evidence for autophagy due to stable phosphorylation of ULK1 Ser757, but in the TamR context there was an increase of phosphorylation of AMPKα Thr137, a decrease in phosphorylation of ULK1 Ser757, and an increase in the levels of LC3 I and a decrease in Beclin1[51] **(Fig 3.11A)**. The results in the TamR T47D when treated with *cis*-RSV are consistent with the decrease of mTORC1 phosphorylation seen in **Figure 3.10**. It can be concluded from this data that treatment with *cis*-RSV leads to a decrease in mTOR signaling and an increase in autophagy in the TamR T47D context. In the WT T47D context, *trans*-RSV has characteristic features of autophagy induction signified by the increase in phosphorylation of AMPKα Thr137, a decrease in phosphorylation of ULK1 Ser 757, increased ratio of LC3 II/LC3I and decrease in the presence of Beclin1. The increased ratio of LC3II/LCI in the WT *trans*-RSV treatment is the most evident of the four treatment scenarios and as LC3II is a late-stage protein that occurs as the autophagosome has almost formed serves as evidence to support that autophagy induced by *trans*-RSV occurs at 24 hr[52]. However, the relationship between *trans*-RSV and autophagy is altered in the TamR T47D. While there remains an increase in expression of p-AMPKα, p-ULK1 levels have stabilized to control values, Beclin1 values have stabilized compared to control and there is a lesser presence of LC3II than in the WT context **(Fig 3.11B)**. These data support that autophagy plays a role in the unique response of *cis*-RSV in the TamR T47D, whereas the

loss of autophagy signaling in TamR T47D with *trans*-RSV supports that the growth inhibitory effects of *trans*-RSV are independent of autophagy. Further pathway analysis was needed to determine the unique effect *trans*-RSV has in promoting growth inhibition.

3.3.3 trans-RSV Inhibits TyrRS Mediated PARP1 Activation

As discussed earlier it was shown that *cis*-RSV bound TyrRS activates PARP1 and *trans*-RSV prevents TyrRS mediated PARP1 activation. However, our previous work used natural RSV and did not explicitly use treatments with *cis*- and *trans*-RSV[40]. Therefore, we treated WT MCF-7 with *cis*- or *trans*-RSV and processed the samples for a PARP1 IP. Treatment with *cis*-RSV maintained basal levels of TyrRS interaction with and activation of PARP1. Treatment with *trans*-RSV was shown to prevent TyrRS interaction with and activation of PARP1 **(Fig 3.12)**. This loss of TyrRS mediated PARP1 activation after treatment with *trans*-RSV lead to the analysis of the effects of *cis*- and *trans*-RSV on DNA Damage signaling.

3.3.4 trans-RSV Induced DDR Signaling

trans-RSV is known to activate both p53 and the DDR through DNA damage[53,54]. *cis*-RSV also has the potential to be involved in DDR signaling through activation of PARP1[40]. It was hypothesized that *trans*-RSV would induce DNA damage in all contexts and *cis*-RSV would not induce DNA damage, but mediate activation of p53. DDR signaling was tested in WT and TamR T47D that were treated with either Tam or *cis*- or *trans*-RSV alone and in combination with Tam. This Western Blot assay displays a distinct difference in DDR between both *cis*-RSV and *trans*-RSV treatments, particularly in WT T47D.

Treatment with *cis*-RSV in and a combination of *cis*-RSV and Tam in did not change the level or decreased levels of phosphorylation of H2A.X Ser139 in the WT context. *cis*-RSV alone and in combination with Tam experienced no increase in phosphorylation of the DSB marker, CHK2 Thr68, building a case for *cis*-RSV to induce growth inhibition independent of DNA damage in WT T47D. *cis*- alone and *cis*-RSV in combination with Tam both experienced decreases in phosphorylation of H3 Ser10. p53, another marker for DNA damage, was phosphorylated at the Ser15 site in both WT and TamR T47D when treated with *cis*-RSV. Maintenance of the activation of PARP1 may explain the activation of p53 by *cis*-RSV treatment **(Fig 3.13A)**. *trans*-RSV and the combination of *trans*-RSV and Tam resulted in an increase in phosphorylation of H2A.X Ser139 which is indicative of DSB. In addition to H2A.X Ser139 another DSB marker, CHK2 Thr68, provided additional evidence for DSB occurrence in *trans*-RSV treatment. The decrease in H3 Ser10 protein expression in *trans*- and *trans-RSV* and Tam combination in both the WT and TamR cells indicates either a decrease in the formation of R loops or possibly the prevention of R loop resolution by condensation through phosphorylation of H3[55]. p53 was phosphorylated at Ser15 during *trans*-RSV treatment which should be related to the increase in phosphorylation of DSB markers, H2A.X Ser139 and CHK2 Thr68 **(Fig 3.13B)**. From this set of experiments, it can be determined that *cis*-RSV does not induce DDR signaling through DNA damage in WT T47D but may increase DNA damage repair signaling from the activation of p53, and in the TamR context *cis*-RSV may have activated the DDR response through the increase in phosphorylation of H2A.X Ser139. *trans*-RSV induced the DDR

response in both WT and TamR T47D providing evidence that growth inhibition induced by *trans*-RSV is related to DNA damage.

Table 3.1. Hormone receptor status of breast cancer cell lines.

Cell Line	ERα	PR	HER2
BT-474[56]	+	+	+
MCF-7[56]	+	+	-
T47D[56]	+	+	-
HCC1954[56]	-	-	+
SK-BR-3[56]	-	-	+
JIMT-1[57]	-	-	+

Table 3.2 IC50 Values of *cis*- and *trans*-RSV in all cells evaluated in the study.

Cell Line	*cis*-RSV (μM)	*trans*-RSV (μM)	*cis*-RSV+Tam (μM)	*trans*-RSV+Tam (μM)
WT T47D	114.94	58.97	88.99	29.00
TamR T47D	79.31	61.36	61.01	52.08
WT MCF-7	206.21	63.70	99.83	71.22
TamR MCF-7	174.11	42.61	86.96	49.76
HCC1954	46.02	65.88	N/A	N/A
JIMT-1	324.45	122.11	N/A	N/A
BT-474	359.72	431.68	N/A	N/A
SK-BR-3	703.88	730.54	N/A	N/A

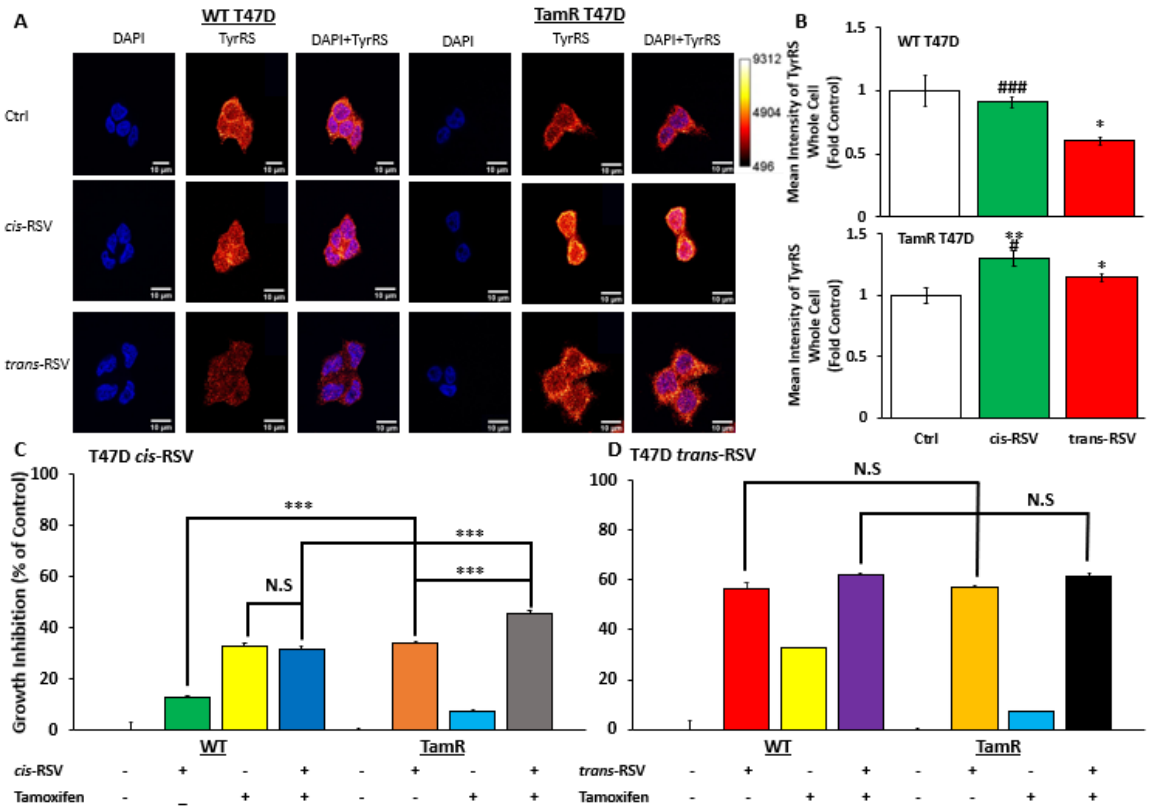

Figure 3.1. Stabilization of TyrRS enhances the growth inhibitory effect of *cis*-RSV in TamR T47D (A) WT and TamR T47D were treated with either *cis*- or *trans*-RSV (50 µM) for 1 hr on coverslips. Coverslips were stained with primary anti-TyrRS, and secondary Alexa Fluor 488, mounted to coverslips with DAPI and imaged with Carl Zeiss LSM700 Confocal Microscope. A calibration bar is used to represent the brightness of the signal obtained by the TyrRS protein and the scale bar represents 10 µM on each image. **(B)** Images were quantified with Protein_Expression_and_Colocalization script to produce graphs for the mean intensity of TyrRS protein in both WT and TamR T47D that show change as fold higher or lower than the control. Quantification was done using 15-49 cells per treatment. **(C)** WT and TamR T47D were treated either alone or in combination with 50 µM *cis*-RSV and 5 µM Tam for 72 hr with growth inhibition values recorded with Promega Titer Assay. **(D)** WT and TamR T47D were treated either alone or in combination with 50 µM trans-RSV and 5µM Tam for 72 hr with growth inhibition values recorded with Promega Titer Assay. Growth inhibition treatments were performed using n=5 technical repeats. All growth inhibition values are represented as % fold higher or lower than the control. The standard error of the mean is represented by the error bars. Statistical difference between the control and treatment values for immunofluorescence was determined from a one-way ANOVA, post hoc Tukey Kramer Test and student's t-test. Statistical difference between the control and treatment values for growth inhibition was determined by the student's

t-test and are indicated by asterisks (*p<0.05, **p<0.01, ***p<0.001) or N.S as no significance. Asterisk key for immunofluorescence *=difference from control, #=difference between *cis*- and *trans*-RSV.

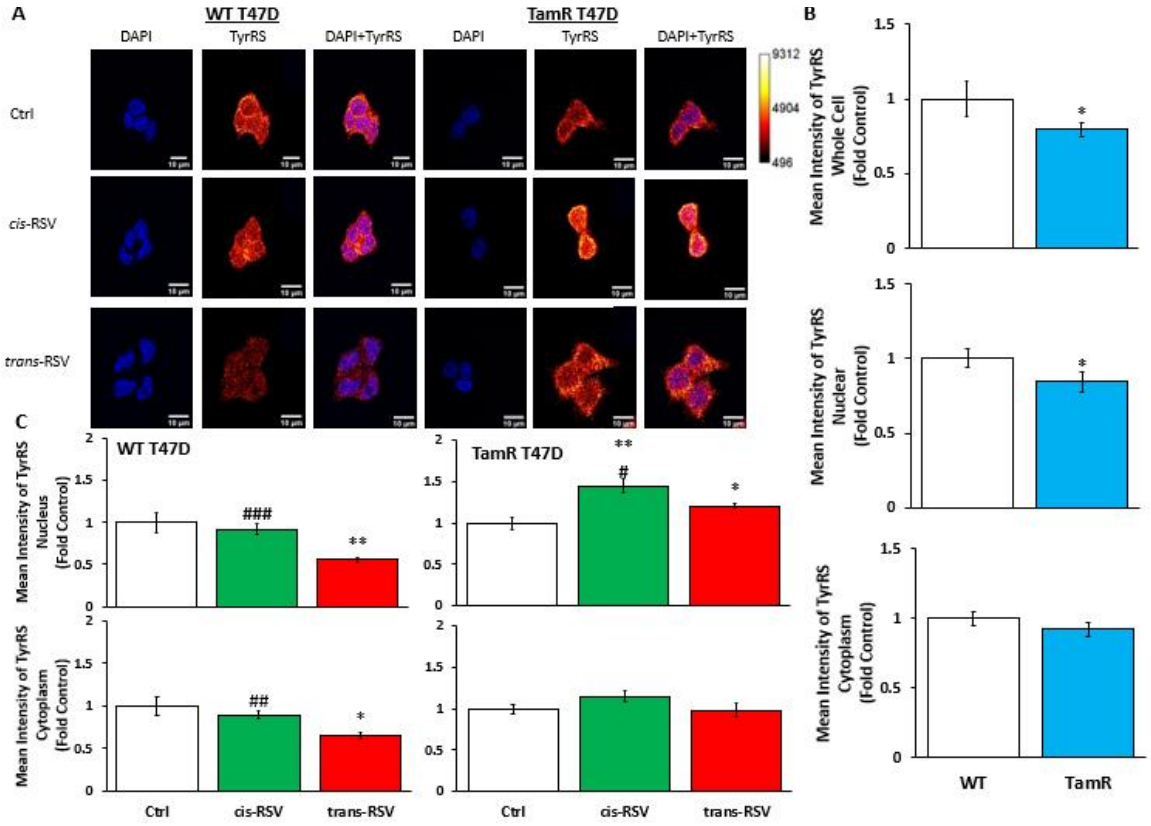

Figure 3.2. Effect of *cis*- and *trans*-RSV on the localization of TyrRS protein and differences in WT and TamR T47D TyrRS localization. (A) WT and TamR T47D were treated with either *cis*- or *trans*-RSV (50 µM) for 1 hr on coverslips. Coverslips were stained with primary anti-TyrRS, and secondary Alexa Fluor 488, mounted to coverslips with DAPI and imaged with Carl Zeiss LSM700 Confocal Microscope. The calibration bar is used to represent the brightness of the signal obtained by the TyrRS protein and the scale bar represents 10 µM on each image. Images are representative of the whole set. **(B)** Images were quantified with Protein_Expression_and_Colocalization script to produce graphs for the mean intensity of TyrRS to compare both total, nuclear, and cytoplasmic protein expression in WT and TamR T47D as a fold comparison of the control. Quantification was done using 15-49 cells per treatment. **(C)** Differences in TyrRS protein localization in nucleus and cytoplasm after treatment *cis*- and *trans*-RSV in WT and TamR T47D are displayed as graphs and all treatments are compared as a fold to the control. The standard error of the mean is represented by the error bars. Statistical difference between the control and treatment values for immunofluorescence was determined from a one-way

ANOVA, post hoc Tukey Kramer Test and student's t-test are indicated by asterisks (*p<0.05, **p<0.01, ***p<0.001). Asterisk key for immunofluorescence *= difference from control, #=difference between *cis*- and *trans*-RSV.

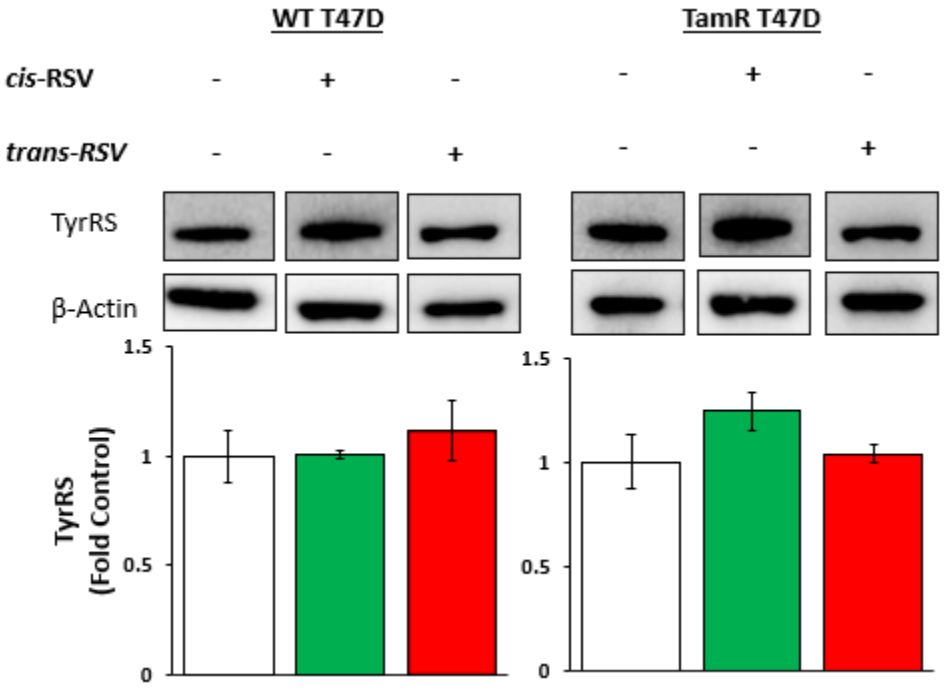

Figure 3.3. Stabilization of TyrRS in T47D when treated with *cis*-RSV. WT and TamR T47D were treated with 50 µM *cis*-RSV for 24 hr and processed for TyrRS in Western Blots. All treatments performed n=3, with each blot shown being a representation of the whole. Blots were quantified to produce graphs displaying protein expression of each treatment as a fold comparison to the control.

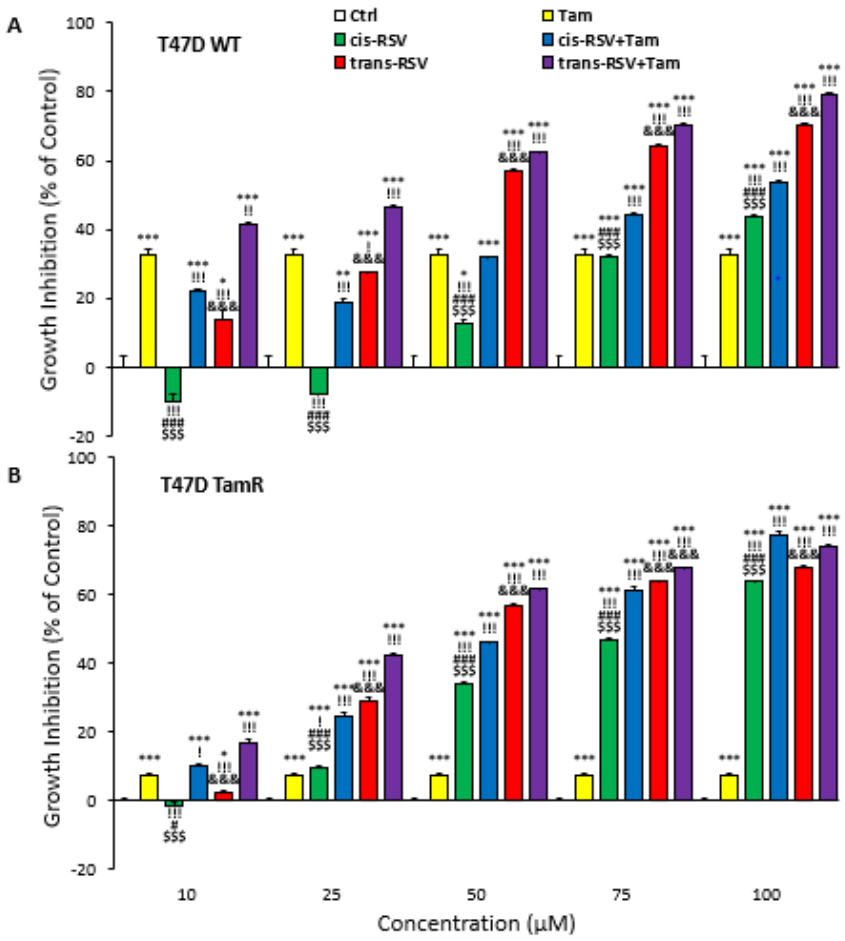

Figure 3.4. Growth inhibition dose response of cis- and trans-RSV in WT and TamR T47D. (A-B) WT and TamR T47D were treated with increasing concentrations of *cis*- or *trans*-RSV for 72 hr alone or in combination with (5 μM) Tam. Growth inhibition values were recorded with Promega Titer Assay. Growth inhibition treatments were performed using n=5 technical repeats. All values are represented as % fold higher or lower than the control. The standard error of the mean is shown by the error bars and differences in cell viability were compared by a two-tailed equal variance student's t-test and are indicated by asterisks (*p<0.05, **p<0.01, ***p<0.001). *=difference between control and treatment, !=difference between treatment and Tam, #=difference between *cis*- and *trans*-RSV, $=difference between *cis*-RSV and *cis*-RSV + Tam, &=difference between *trans*-RSV and *trans*-RSV + Tam.

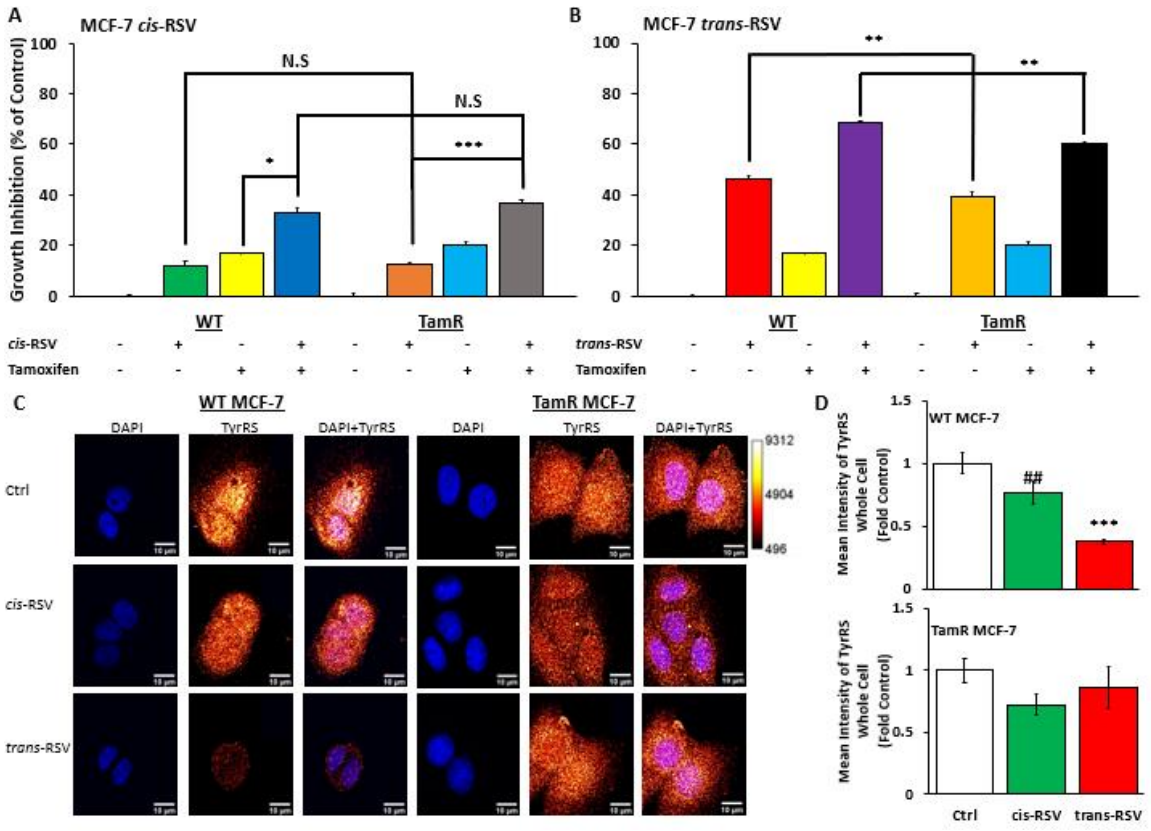

Figure 3.5. Effect of *cis*- and *trans*-RSV on the expression of TyrRS protein and growth inhibition in WT and TamR MCF-7. (A) WT and TamR MCF-7 were treated either alone or in combination with 50 µM *cis*-RSV and 5 µM Tam for 72 hr with growth inhibition values recorded with Promega Titer Assay. **(B)** WT and TamR MCF-7 were treated either alone or in combination with 50 µM trans-RSV and 5µM Tam for 72 hr with growth inhibition values recorded with Promega Titer Assay. Growth inhibition treatments were performed using n=4 technical repeats. All growth inhibition values are represented as % fold higher or lower than the control. **(C)** WT and TamR MCF-7 were treated with either *cis*- or *trans*-RSV (50 µM) for 1 hr on coverslips. Coverslips were stained with primary anti-TyrRS, and secondary Alexa Fluor 488, mounted to coverslips with DAPI and imaged with Carl Zeiss LSM700 Confocal Microscope. The calibration bar is used to represent the brightness of the signal obtained by the TyrRS protein and the scale bar represents 10 µM on each image. Images are representative of the whole set. **(D)** Images were quantified with Protein_Expression_and_Colocalization to produce graphs for the mean intensity of TyrRS protein in both WT and TamR MCF-7. Quantification was performed using 10-21 cells per treatment. The standard error of the mean is represented by the error bars. Statistical difference between the control and treatment values for growth inhibition was determined by the student's t-test with significance denoted by asterisks (*p<0.05, **p<0.01, ***p<0.001) or N.S as no significance. Statistical difference between the control

and treatment values for immunofluorescence was determined from a one-way ANOVA, post hoc Tukey Kramer Test and student's t-test with significance denoted by asterisks (*p<0.05, **p<0.01, ***p<0.001). Asterisk key for immunofluorescence *= difference from control, #=difference between *cis*- and *trans*-RSV.

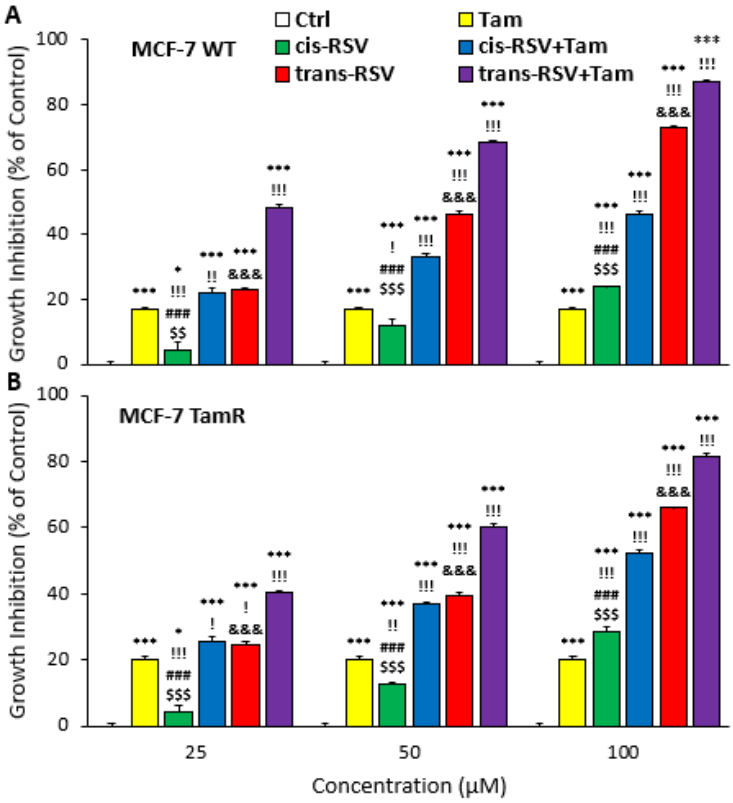

Figure 3.6. Growth inhibition dose response of cis- and trans-RSV in WT and TamR MCF-7. (A-B) WT and TamR MCF-7 were treated with increasing concentrations of *cis*- or *trans*-RSV for 72 hr alone or in combination with (5 μM) Tam for WT **(A)** and (7.5μM) Tam for TamR **(B)**. Growth inhibition values were recorded with Promega Titer Assay. Experiments were performed to n=4 technical replicates. All values are represented as % fold higher or lower than the control. The standard error of the mean is shown by the error bars and differences in cell viability were compared by the student's t-test and are indicated by asterisks (*p<0.05, **p<0.01, ***p<0.001). *=difference between control and treatment, !=difference between treatment and Tam, #=difference between *cis*- and *trans*-RSV, $=difference between *cis*-RSV and *cis*-RSV + Tam, &=difference between *trans*-RSV and *trans*-RSV + Tam.

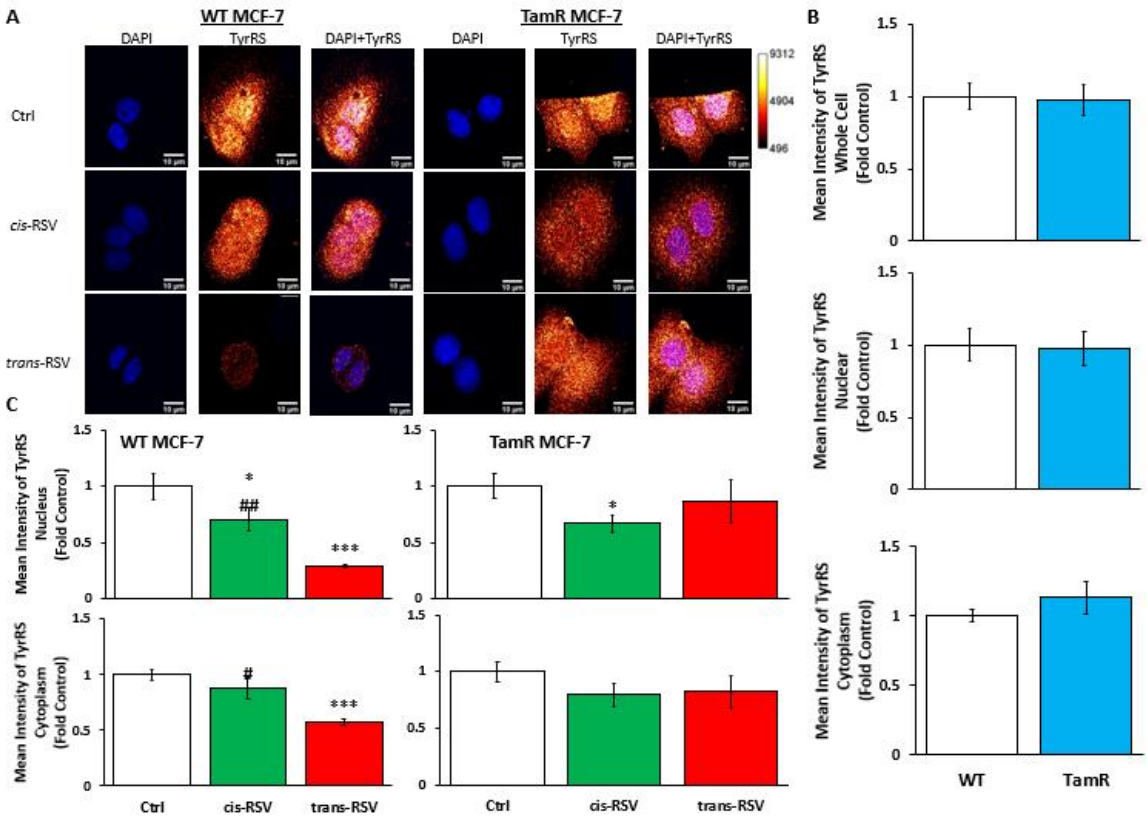

Figure 3.7. Effect of *cis*- and *trans*-RSV on the localization of TyrRS protein and differences in WT and TamR MCF-7 TyrRS localization. (A) WT and TamR MCF-7 were treated with either *cis*- or *trans*-RSV (50 µM) for 1 hr on coverslips. Coverslips were stained with primary anti-TyrRS, and secondary Alexa Fluor 488, mounted to coverslips with DAPI and imaged with Carl Zeiss LSM700 Confocal Microscope. The calibration bar is used to represent the brightness of the signal obtained by the TyrRS protein, and the scale bar represents 10 µM on each image. **(B)** Images were quantified with Protein_Expression_and_Colocalization to produce graphs for the mean intensity of TyrRS to compare both total, nuclear, and cytoplasmic protein expression in WT and TamR MCF-7 as a fold comparison of the control. Quantification was performed using 10-21 cells per treatment. **(C)** Differences in TyrRS protein localization in nucleus and cytoplasm after treatment *cis*- and *trans*-RSV in WT and TamR MCF-7 are displayed as graphs and all treatments are compared as a fold to the control. , The standard error of the mean, is represented by the error bars. Statistical difference between the control and treatment values for immunofluorescence were determined from a one-way ANOVA, post hoc Tukey Kramer Test and student's t-test are indicated by asterisks (*p<0.05, **p<0.01, ***p<0.001) Asterisk key for immunofluorescence *= difference from control, #=difference between *cis*- and *trans*-RSV.

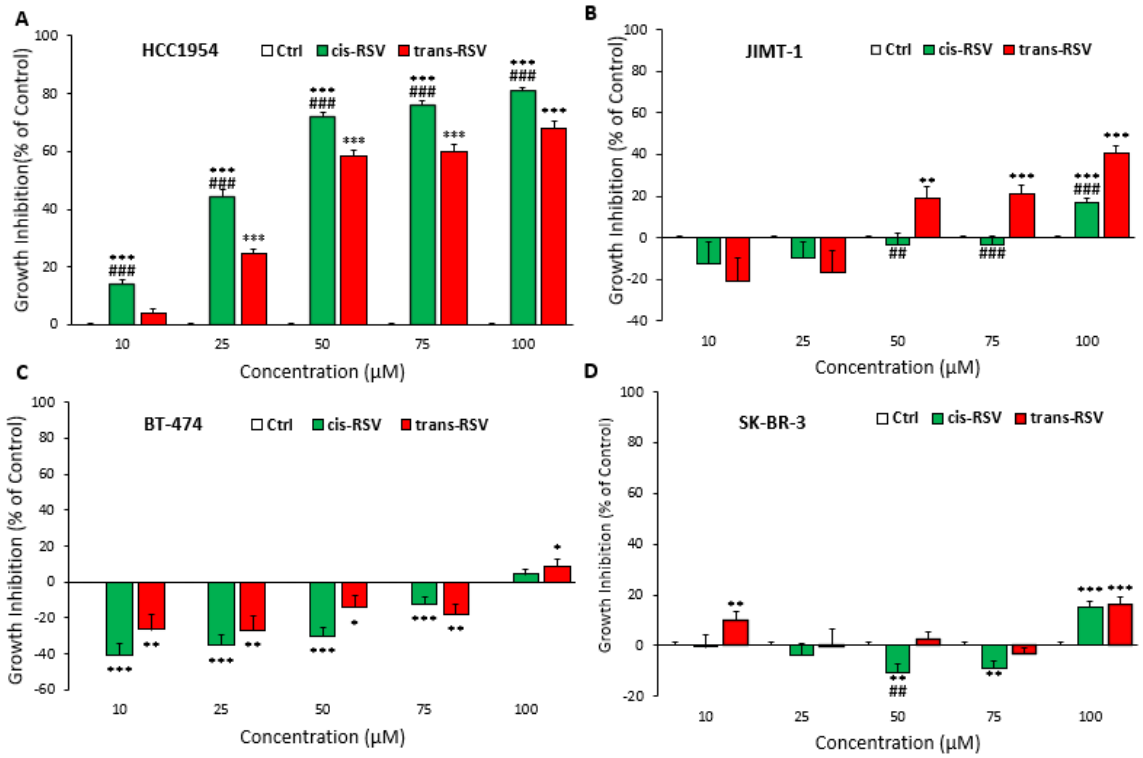

Figure 3.8 Dose response of cis- and trans-RSV shows *cis*-RSV has a greater growth inhibitory effect in HCC1954 than *trans*-RSV. (A) HCC1954, **(B)** JIMT-1, **(C)** BT-474, **(D)** SK-BR-3, were treated with increasing concentrations of *cis*- or *trans*-RSV for 72 hr and growth inhibition values were recorded with MTT assay. HCC1954 and JIMT-1 cells were performed to n=5 while BT-474 and SK-BR-3 were performed to n=3. All values are represented as % fold higher or lower than the control. Standard error of the mean is shown by the error bars and differences in growth inhibition were compared by the student's t-test and are indicated by asterisks (*p<0.05, **p<0.01, ***p<0.001). *=difference between treatment and control. #=difference between *cis*- and *trans*-RSV.

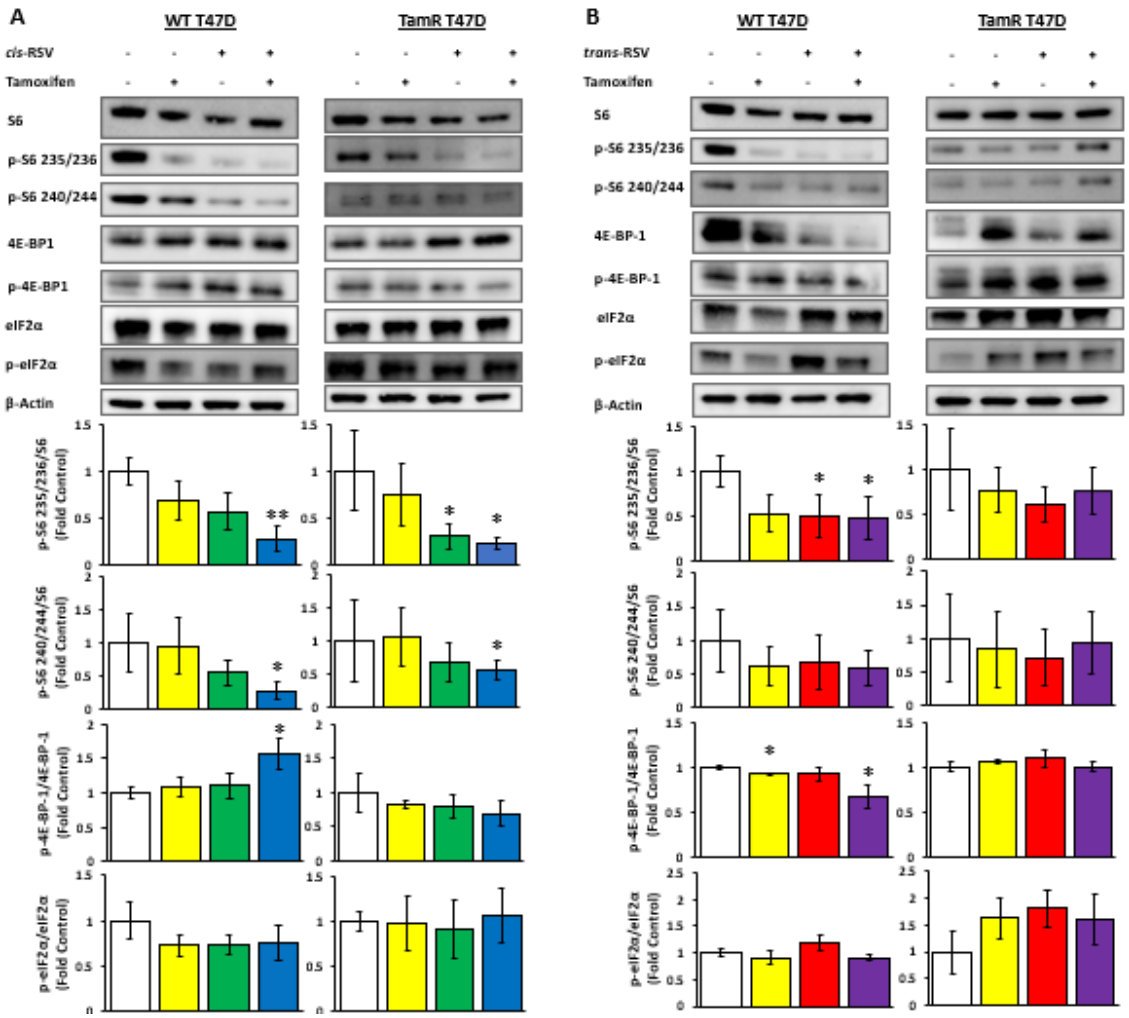

Figure 3.9. Treatment with *cis*- and *trans*-RSV inhibit protein synthesis signaling. T47D (WT and TamR) were treated with either Tam (5 µM)or *cis* (**A**)-or *trans* (**B**)-RSV (50 µM) alone and in combination with Tam for 24 hr and were analyzed for S6 Ribosomal Protein, phospho-S6 Ser235/236, phospho-S6 Ser240/244, 4E-BP-1, phospho-4E-BP-1 Thr37/46, eIF2α and phospho-eIF2α Ser51 for Western Blot. All treatments were performed to n=3 apart from eIF2α and phospho-eIF2α Ser51, which were performed to n=2. Each blot shown is a representation of the whole. Blots were quantified to produce graphs displaying protein expression of each treatment as a fold comparison to the control. The standard error of the mean is represented by the error bars. Statistical difference between the control and treatment values was determined from a one-way ANOVA, post hoc Tukey Kramer Test and student's t-test. Statistical significance from control is indicated by asterisks (*p<0.05, **p<0.01, ***p<0.001). β-Actin, from **Figure 3.3** was adapted and used in **Figure 3.9** as all blots presented in both figures are of the same experimental group.

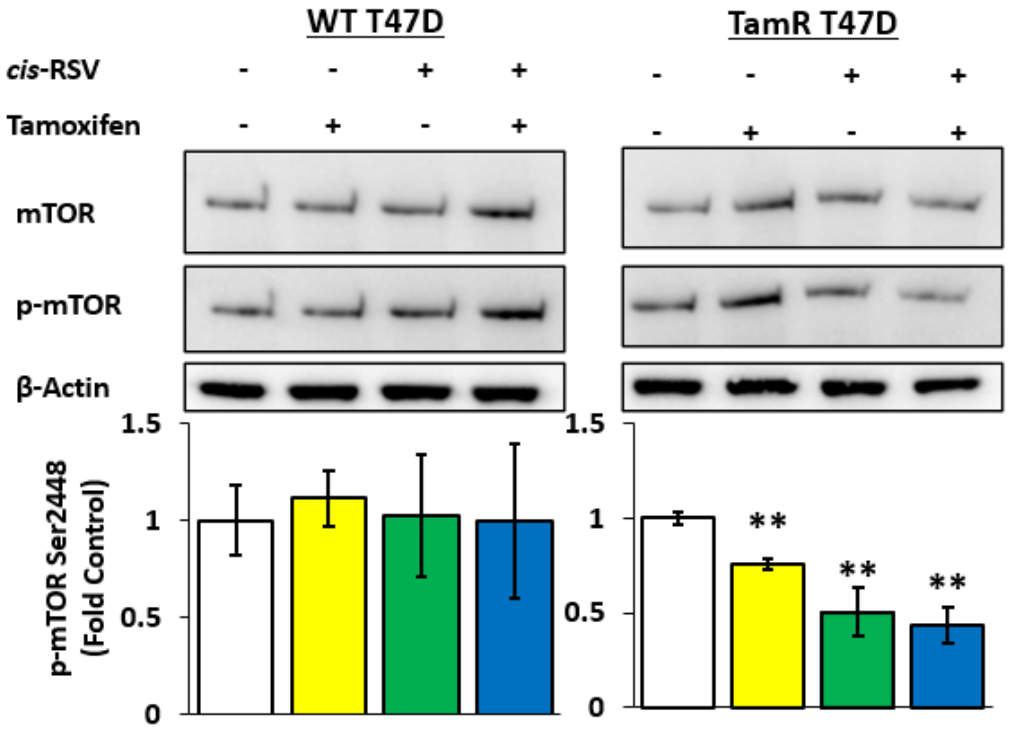

Figure 3.10. Loss of mTOR signaling from treatment with *cis*-RSV in TamR T47D. WT and TamR T47D were treated with 50 µM *cis*-RSV for 24 hr and processed for mTOR and phospho-mTOR Ser2448 in Western Blots. All treatments were performed to n=3, with each blot shown is a representation of the whole. Blots were quantified to produce graphs displaying protein expression of each treatment as a fold comparison to the control. Statistical difference between the control and treatment values was determined from a one-way ANOVA, post hoc Tukey Kramer Test and student's t-test based on ANOVA results. Statistical significance from control is indicated by asterisks (*p<0.05, **p<0.01, ***p<0.001). β-Actin, from **Figure 3.3** was adapted and used in **Figure 3.10** as all blots presented in both figures are of the same experimental group.

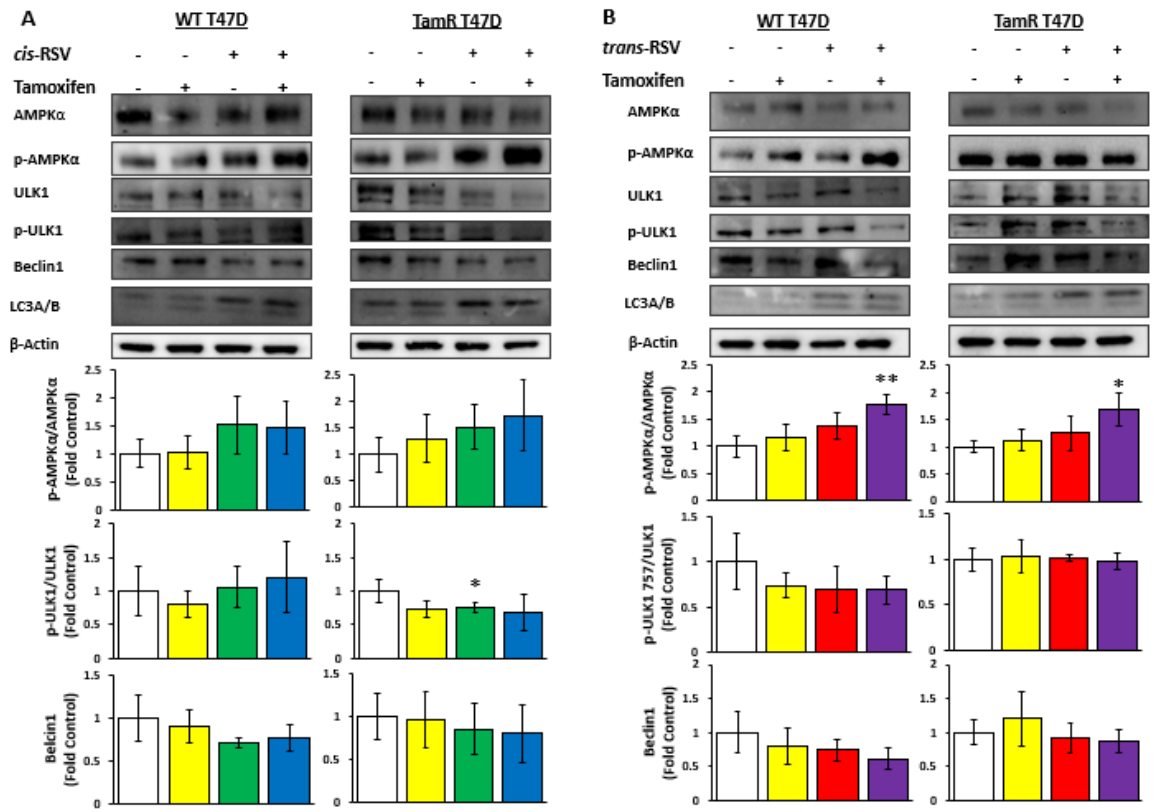

Figure 3.11. Distinct effects of *cis*- and *trans*-RSV on autophagy signaling. T47D (WT and TamR) were treated with either Tam (5 µM) or *cis* (**A**)-or *trans* (**B**)-RSV (50 µM) alone and in combination with Tam for 24 hr and were analyzed for AMPKα, phospho-AMPKα Thr172, ULK1, phospho-ULK1 Ser757, Beclin1 and LC3A/B for Western Blot. All treatments were performed to n=3, with each blot shown is a representation of the whole. Blots were quantified to produce graphs displaying protein expression of each treatment as a fold comparison to the control. The standard error of the mean is represented by the error bars. Statistical difference between the control and treatment values was determined from a one-way ANOVA, post hoc Tukey Kramer Test and student's t-test. Statistical significance from control is indicated by asterisks (*p<0.05, **p<0.01, ***p<0.001). β-Actin, from **Figure 3.3** was adapted and used in **Figure 3.11** as all blots presented in both figures are of the same experimental group.

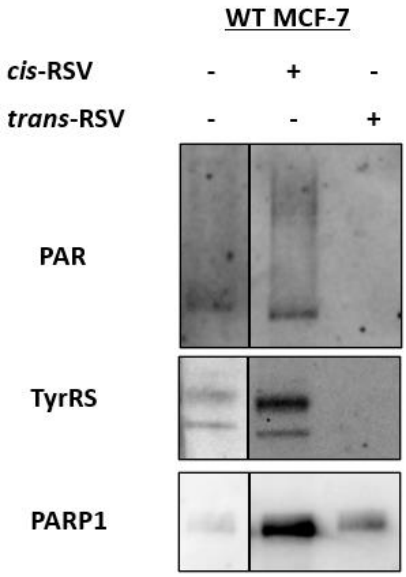

Figure 3.12. *trans*-RSV inhibits TyrRS mediated PARP1 activation. WT MCF-7 were treated with 50 µM *cis*- or *trans*-RSV for 1 hr and processed for PARP1 IP and probed with, Oligo-ADP-Ribose (PAR), TyrRS and PARP1 antibodies.

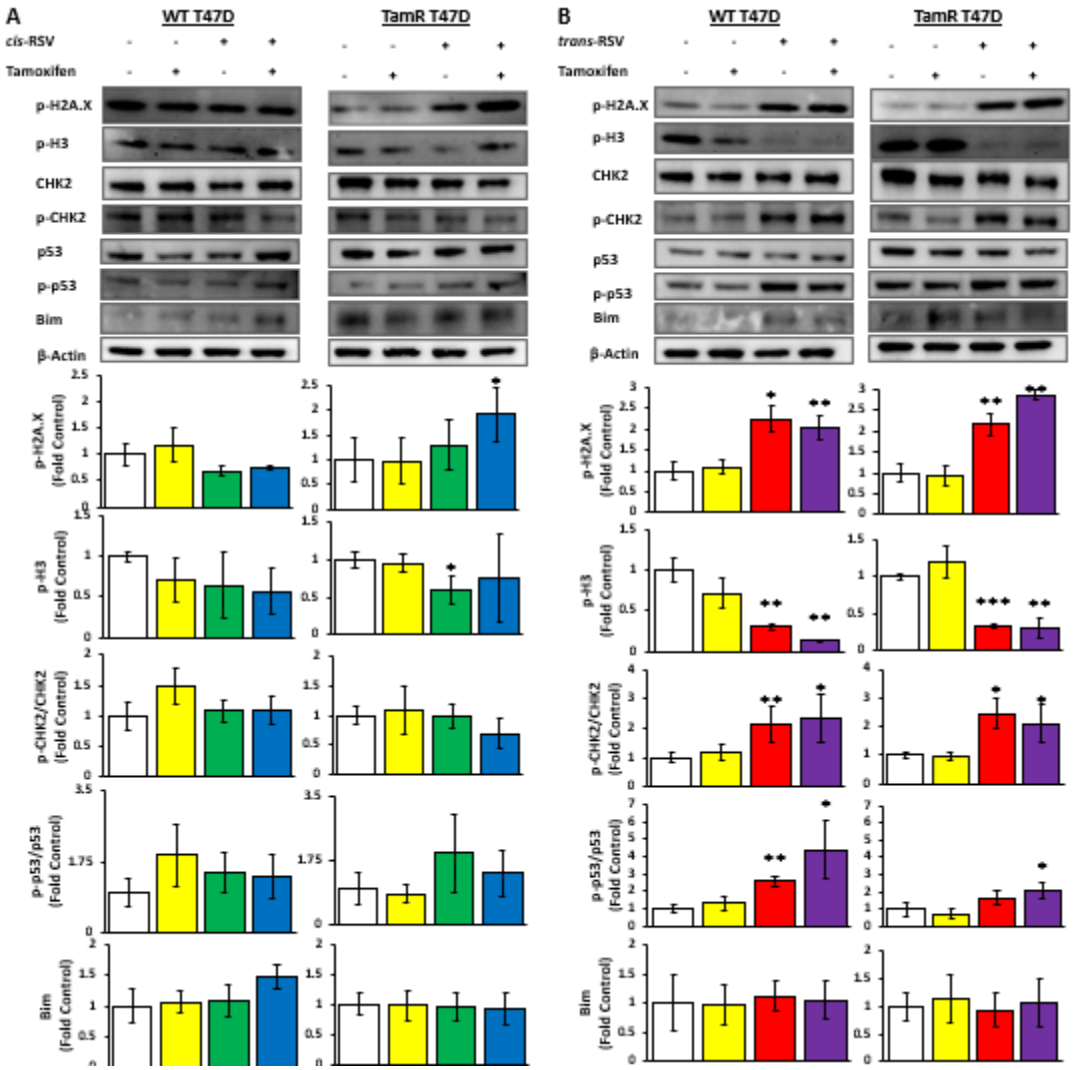

Figure 3.13. *trans*-RSV activates DNA damage response signaling in both WT and TamR T47D. T47D (WT and TamR) were treated with either Tam (5 µM)or *cis* (**A**)-or *trans* (**B**)-RSV (50 µM) alone and in combination with Tam for 24 hr and were analyzed for phospho-H2A.X Ser 139, phospho-H3 Ser10, CHK2, phospho-CHK2 Thr68, Bim, p53 and phospho-p53 Ser15 for Western Blot. All treatments were performed to n=3, with each blot shown is a representation of the whole. Blots were quantified to produce graphs displaying protein expression of each treatment as a fold comparison to the control. The standard error of the mean is represented by the error bars. Statistical difference between the control and treatment values was determined from a one-way ANOVA, post hoc Tukey Kramer Test and student's t-test based on ANOVA results. Statistical significance from control is indicated by asterisks (*p<0.05, **p<0.01, ***p<0.001). β-Actin, from **Figure 3.3** was adapted and used in **Figure 3.13** as all blots presented in both figures are of the same experimental group.

Chapter 4

Discussion

Breast cancer is one of the most common breast cancers that women develop, specifically breast cancers with overexpression of ERα. Typically Tam is used to treat patients who overexpress ERα, however, 30% of all patients treated with Tam will develop resistance to Tam[58]. RSV is a polyphenol found in plants such as grapes and is present in two different isomers, *cis*- and *trans*-RSV. *trans*-RSV was investigated initially for cardioprotective qualities and later anti-cancer effects[20,21]. It was reported that *trans*-RSV was an inhibitor of PDE4D and that TamR cells could be sensitized to Tam or eliminated through PDE4D inhibition[34,35]. In addition to this, it is known that *cis*-RSV can bind to TyrRS and promote PARP1 activation, which can improve genetic stability and decrease cAMP levels through PDE inhibition[40,59]. Therefore, it was proposed that treating TamR cells with either *cis*- or *trans*-RSV would either sensitize or eliminate TamR cells.

This study suggests that *trans*-RSV is may not be a direct inhibitor of PDE4D and contradicts what is stated in the literature[32]. Growth inhibition assays performed in the WT and TamR T47D display that trans-RSV has the same growth-inhibitory capabilities, whether it is in the WT or TamR and the WT and TamR MCF-7 *trans*-RSV has a decreased growth inhibitory effect in the TamR compared to the WT MCF-7. The data suggests that *trans*-RSV may not be a PDE4D inhibitor as a true PDE4D inhibitor would have a

higher growth inhibitory effect when combined with Tam in TamR cells of all contexts[35]. The findings of this study also contradict earlier findings where *trans*-RSV is reported to be a direct SIRT1 activator. If *trans*-RSV were a true SIRT1 activator phosphorylation p53 Ser15 would not have increased as SIRT1 is an inhibitor of p53; however, our study reported that both isoforms of RSV increased phosphorylation of p53 Ser15[19]. This result suggests that both *cis*- and *trans*-RSV are inhibitors of SIRT1. From the growth inhibition analysis of HCC1954 it can be determined that neither *cis*- or *trans*-RSV inhibit cell growth in an ERα dependent manner as HCC1954 is an ERα negative cell line, however this does not rule out the potential for either of the compounds to interact with ERα in a specific context.

The combination of *cis*-RSV and Tam and Tam treatment in WT T47D and *cis*-RSV treatment in TamR T47D have no difference in the ability to inhibit cancer growth, while the combination of *cis*-RSV and Tam in TamR T47D has the highest growth inhibition. Cell signaling analysis in the WT T47D cells revealed that there is no activation of DNA damage signaling by the addition of *cis*-RSV. These promising results suggest that the co-treatment of Tam and *cis*-RSV may prevent the development of TamR or would be a useful treatment in patients who develop TamR cells as the combination of these compounds would provide a growth inhibitory effect in the WT cell line that is independent of DNA damage.

Immunofluorescent imaging, western blotting and IP appear to have shown that the primary pathway that *trans*-RSV uses to induce cell death is from the DNA damage signaling pathway. Loss of TyrRS mediated activation of PARP1 shown by IP was the first indication that *trans*-RSV effects DNA damage signaling. Moreover, *trans*-RSV promoted

the DNA Damage signaling pathway both alone and in combination with Tam as there was a remarkable increase in the amount of phosphorylated H2A.X Ser139, CHK2 Thr68 and p53 Ser15 and inhibited ribosomal translation signaling through the decrease in phosphorylation of S6 Ribosomal Protein Ser240/244 and Ser235/236 sites. This combination of results is confirmed by the literature providing further evidence for *trans*-RSV acting as a DNA damaging compound[54].

Immunofluorescent imaging, growth inhibition assays and western blots suggest that the cytotoxic potential of *cis*-RSV, specifically in TamR T47D, is related to increased TyrRS protein level, inhibition of ribosomal translation and the increased autophagic potential through loss of mTORC1 signaling. Critical indicators of these findings are the increased protein expression of TyrRS after 1 hr of *cis*-RSV treatment, the decreased phosphorylation of S6 Ribosomal Protein Ser240/244 and Ser235/236 sites for protein translation. In conjunction with the decrease in phosphorylation of S6 Ser240/244, the decrease in phosphorylation of 4E-BP-1 Thr37/46 and ULK1 Ser757, the increase in phosphorylation of AMPKα Thr172 and the decrease in phosphorylation of mTOR Ser2448 is indicative of the loss of mTOR activity in *cis*-RSV treated TamR T47D.

Further testing that should be done with *trans*-RSV includes comet assays to confirm DNA damage signaling and the severity of the DNA damage compared to other compounds such as doxorubicin or cisplatin and in comparison, to *cis*-RSV. As it does not appear that *trans*-RSV is a true PDE4D inhibitor it would be interesting to see if *trans*-RSV stimulates the production of cAMP through adenylate cyclase and how that is changed between the WT and TamR context. This experiment could also be applied to *cis*-RSV as

it is possible that *cis*-RSV can indirectly inhibit PDE4D in TamR T47D through TyrRS dependent activation of PARP1. As PARP1 creates more ADP, PDE4D will begin to hydrolyze ADP in addition to cAMP causing AMP levels to increase in the cell. To determine whether only TyrRS total protein level or localization of the TyrRS protein in the nucleus is an essential part of *cis*-RSV activation TamR T47D cells could be transfected with mutant TyrRS that effectively acts as a knockdown to prevent TyrRS acetylation and entry into the nucleus[60]. Other experiments that could be performed to make the study more robust are using qPCR analysis to detect change in mRNA levels of TyrRS after treatment with *cis*- and *trans*-RSV, understand the effect of *cis*- and *trans*-RSV on gene expression though microarray analysis and determining the effects of E2 and Tam both alone and in combination with *cis*- and *trans*-RSV.

Biblography

1 Lumachi F. Current medical treatment of estrogen receptor-positive breast cancer. *World J Biol Chem* 2015;**6**:231. https://doi.org/10.4331/wjbc.v6.i3.231.

2 Nass N, Kalinski T. Tamoxifen resistance: From cell culture experiments towards novel biomarkers. *Pathol Res Pract* 2015;**211**:189–97. https://doi.org/10.1016/j.prp.2015.01.004.

3 Shagufta, Ahmad I. Tamoxifen a pioneering drug: An update on the therapeutic potential of tamoxifen derivatives. *Eur J Med Chem* 2018;**143**:515–31. https://doi.org/10.1016/j.ejmech.2017.11.056.

4 Hu R, Hilakivi-Clarke L, Clarke R. Molecular mechanisms of tamoxifen-associated endometrial cancer (Review). *Oncol Lett* 2015;**9**:1495–501. https://doi.org/10.3892/ol.2015.2962.

5 Jackson SP, Bartek J. The DNA-damage response in human biology and disease. *Nature* 2010;**461**:1071–8. https://doi.org/10.1038/nature08467.The.

6 Sheila D, O'Shea V, Kundu S. Base Excision Repair of Oxidative DNA Damage. *Nature* 2007;**447**:941–50. https://doi.org/10.1038/nature05978.

7 Chaundhuri AR, Nussenzweig A. Multifaceted roles of PARP1 in DNA repair and chromatin remodelling. *Nat Rev Mol Biol* 2017;**18**:610–21. https://doi.org/10.1038/nrm.2017.53.

8 Podhorecka M, Skladanowski A, Bozko P. H2AX phosphorylation: Its role in DNA damage response and cancer therapy. *J Nucleic Acids* 2010;**2010**:. https://doi.org/10.4061/2010/920161.

9 Krejci L, Altmannova V, Spirek M, Zhao X. Homologous recombination and its regulation. *Nucleic Acids Res* 2012;**40**:5795–818. https://doi.org/10.1093/nar/gks270.

10 Bartek J, Lukas J, Bartkova J. DNA damage response as an anti-cancer barrier: Damage threshold and the concept of 'conditional haploinsufficiency'. *Cell Cycle* 2007;**6**:2344–7. https://doi.org/10.4161/cc.6.19.4754.

11 Mizushima N. Autophagy: Process and function. *Genes Dev* 2007;**21**:2861–73. https://doi.org/10.1101/gad.1599207.

12 Mathew R, Karantza-Wadsworth V, White E. Role of Autophagy in Cancer. *Role Autophagy Cancer* 2007;**7**:961–7. https://doi.org/10.5772/55315.

13 Degenhardt K, Mathew R, Beaudoin B, Bray K, Anderson D, Chen G, *et al.* Autophagy promotes tumor cell survival and restricts necrosis, inflammation, and tumorigenesis. *Cancer Cell* 2006;**10**:51–64. https://doi.org/10.1016/j.ccr.2006.06.001.

14 Manuscript A. Metabolic Catastrophe as a means of cell death 2010;**120**:379–83. https://doi.org/10.1242/jcs.03349.Metabolic.

15 Tan TT, Degenhardt K, Nelson DA, Beaudoin B, Nieves-Neira W, Bouillet P, *et al.* Key roles of BIM-driven apoptosis in epithelial tumors and rational chemotherapy. *Cancer Cell* 2005;**7**:227–38. https://doi.org/10.1016/j.ccr.2005.02.008.

16 Karantza-Wadsworth V, Patel S, Kravhuk O, Chen G, Mathew R, Shengkan J, *et al.* Autophagy mitigates metabolic stress and genome damage in mammary tumorigenesis. *Genes Dev* 2007;**21**:1621–35. https://doi.org/10.1101/gad.1565707.fects.

17 Kroemer G, Beth L. Autophagic cell death: the story of a misnomer. *Nat Rev Mol Cell Biol* 2008;**9**:1004–10. https://doi.org/10.1038/jid.2014.371.

18 Shimizu S, Yoshida T, Tsujioka M, Arakawa S. Autophagic cell death and cancer. *Int J Mol Sci* 2014;**15**:3145–53. https://doi.org/10.3390/ijms15023145.

19 Howitz KT, Bitterman KJ, Cohen HY, Lamming DW, Lavu S, Wood JG, *et al.* Small molecule activators of sirtuins extend Saccharomyces cerevisiae lifespan. *Nature* 2003;**425**:191–6. https://doi.org/10.1038/nature01960.

20 Kulkarni SS, Cantó C. The molecular targets of resveratrol. *Biochim Biophys Acta - Mol Basis Dis* 2015;**1852**:1114–23. https://doi.org/10.1016/j.bbadis.2014.10.005.

21 Jang M, Cai L, Udeani GO, Slowing K V., Thomas CF, Beecher CWW, *et al.* Cancer chemopreventive activity of resveratrol, a natural product derived from grapes. *Science (80-)* 1997;**275**:218–20. https://doi.org/10.1126/science.275.5297.218.

22 Cai H, Scott E, Kholghi A, Andreadi C, Rufini A, Karmokar A, *et al.* Cancer chemoprevention: Evidence of a nonlinear dose response for the protective effects of resveratrol in humans and mice. *Sci Transl Med* 2015;**7**:. https://doi.org/10.1126/scitranslmed.aaa7619.

23 Wang R, Zheng Y, Kim H, Xu X, Cao L, Lahusen T, *et al.* Interplay among BRCA1, SIRT1 and Survivin during BRCA1-Associated Tumorigenesis. *Mol Cell* 2009;**32**:11–20. https://doi.org/10.1016/j.molcel.2008.09.011.Interplay.

24 Sun T, Jiao L, Wang Y, Yu Y, Ming L. SIRT1 induces epithelial-mesenchymal transition by promoting autophagic degradation of E-cadherin in melanoma cells article. *Cell Death Dis* 2018;**9**:. https://doi.org/10.1038/s41419-017-0167-4.

25 Elstrodt F, Hollestelle A, Nagel JHA, Gorin M, Wasielewski M, Van Den Ouweland A, *et al.* BRCA1 mutation analysis of 41 human breast cancer cell lines reveals three new deleterious mutants. *Cancer Res* 2006;**66**:41–5. https://doi.org/10.1158/0008-5472.CAN-05-2853.

26 Jin X, Wei Y, Xu F, Zhao M, Dai K, Shen R, *et al.* SIRT1 promotes formation of breast cancer through modulating Akt activity. *J Cancer* 2018;**9**:2012–23. https://doi.org/10.7150/jca.24275.

27 Gehm BD, McAndrews JM, Chien PY, Jameson JL. Resveratrol, a polyphenolic compound found in grapes and wine, is an agonist for the estrogen receptor. *Proc Natl Acad Sci U S A* 1997;**94**:14138–43. https://doi.org/10.1073/pnas.94.25.14138.

28 Gehm BD, Levenson AS, Liu H, Lee EJ, Amundsen BM, Cushman M, *et al.* Estrogenic effects of resveratrol in breast cancer cells expressing mutant and wild-type estrogen receptors: Role of AF-1 and AF-2. *J Steroid Biochem Mol Biol* 2004;**88**:223–34. https://doi.org/10.1016/j.jsbmb.2003.12.002.

29 Nwachukwu JC, Srinivasan S, Bruno NE, Parent AA, Hughes TS, Pollock JA, *et al.* Resveratrol modulates the inflammatory response via an estrogen receptor-signal integration network. *Elife* 2014;**2014**:. https://doi.org/10.7554/eLife.02057.

30 Bhat KPL, Lantvit D, Christov K, Mehta RG, Moon RC, Pezzuto JM. Estrogenic and antiestrogenic properties of resveratrol in mammary tumor models. *Cancer Res* 2001;**61**:7456–63.

31 Fertig B, Baillie G. PDE4-Mediated cAMP Signalling. *J Cardiovasc Dev Dis* 2018;**5**:8. https://doi.org/10.3390/jcdd5010008.

32 Zhao P, Chen SK, Cai YH, Lu X, Li Z, Cheng YK, *et al.* The molecular basis for the inhibition of phosphodiesterase-4D by three natural resveratrol analogs. Isolation, molecular docking, molecular dynamics simulations, binding free energy, and bioassay. *Biochim Biophys Acta - Proteins Proteomics* 2013;**1834**:2089–96. https://doi.org/10.1016/j.bbapap.2013.07.004.

33 El-Mowafy AM, Alkhalaf M. Resveratrol activates adenylyl-cyclase in human breast cancer cells: A novel, estrogen receptor-independent cytostatic mechanism. *Carcinogenesis* 2003;**24**:869–73. https://doi.org/10.1093/carcin/bgg015.

34 Park SJ, Ahmad F, Philp A, Baar K, Williams T, Luo H, *et al.* Resveratrol ameliorates aging-related metabolic phenotypes by inhibiting cAMP phosphodiesterases. *Cell* 2012;**148**:421–33. https://doi.org/10.1016/j.cell.2012.01.017.

35 Mishra RR, Belder N, Ansari SA, Kayhan M, Bal H, Raza U, *et al. Reactivation of cAMP Pathway by PDE4D Inhibition Represents a Novel Druggable Axis for Overcoming Tamoxifen Resistance in ER-positive Breast Cancer*. vol. 24. 2018.

36 Tennen RI, Michishita-Kioi E, Chua KF. Finding a target for resveratrol. *Cell* 2012;**148**:387–9. https://doi.org/10.1016/j.cell.2012.01.032.

37 Gao P, Li N, Ji K, Wang Y, Xu C, Liu Y, *et al.* Resveratrol targets TyrRS acetylation to protect against radiation-induced damage. *FASEB J* 2019;**33**:8083–93. https://doi.org/10.1096/fj.201802474RR.

38 Lakin ND, Jackson SP. Regulation of p53 in response to DNA damage. *Oncogene* 1999;**18**:7644–55. https://doi.org/10.1038/sj.onc.1203015.

39 She QB, Bode AM, Ma WY, Chen NY, Dong Z. Resveratrol-induced activation of p53 and apoptosis is mediated by extracellular-signal-regulated protein kinases and p38 kinase. *Cancer Res* 2001;**61**:1604–10.

40 Sajish M, Schimmel P. A human tRNA synthetase is a potent PARP1-activating effector target for resveratrol. *Nature* 2015;**519**:370–3. https://doi.org/10.1038/nature14028.

41 Pazzaglia S, Pioli C. Multifaceted Role of PARP-1 in DNA Repair and Inflammation : Pathological and Therapeutic Implications in Cancer and Non-Cancer Diseases 2020.

42 Morrison C, Smith G, Stingl L, Jackson S, Wagner E, Wang Z. Genetic Interaction Between PARP and DNA-PK in V(D)J recombination and tumorigensis. *Nature* 1997;**17**:479–82.

43 Navarro J, Gozalbo-López B, Méndez AC, Dantzer F, Schreiber V, Martínez C, *et al.* PARP-1/PARP-2 double deficiency in mouse T cells results in faulty immune responses and T lymphomas. *Sci Rep* 2017;**7**:1–14. https://doi.org/10.1038/srep41962.

44 Zuo H, Yang D, Yang Q, Tang H, Fu YX, Wan Y. Differential regulation of breast cancer bone metastasis by PARP1 and PARP2. *Nat Commun* 2020;**11**:. https://doi.org/10.1038/s41467-020-15429-z.

45 Mo Z, Zhang Q, Liu Z, Lauer J, Shi Y, Sun L, *et al.* Neddylation Requires Glycyl-tRNA synthetase to protect activated E2. *Nat Struct Mol Biol* 2016;**23**:730–7. https://doi.org/10.1016/j.physbeh.2017.03.040.

46 Giegé R. History of tRNA recognition by synthetases. *J Biosci* 2006;**31**:477–88. https://doi.org/10.1007/978-1-4939-6518-2_3.

47 Boulikas T. Poly(ADP-ribose) synthesis and degradation in mammalian nuclei. *Anal Biochem* 1992;**203**:252–8. https://doi.org/10.1016/0003-2697(92)90310-4.

48 Ward A, Balwierz A, Zhang JD, Küblbeck M, Pawitan Y, Hielscher T, *et al.* Re-expression of microRNA-375 reverses both tamoxifen resistance and accompanying EMT-like properties in breast cancer. *Oncogene* 2013;**32**:1173–82. https://doi.org/10.1038/onc.2012.128.

49 Navé BT, Ouwens DM, Withers DJ, Alessi DR, Shepherd PR. Mammalian target of rapamycin is a direct target for protein kinase B: Identification of a convergence point for opposing effects of insulin and amino-acid deficiency on protein translation. *Biochem J* 1999;**344**:427–31. https://doi.org/10.1042/0264-6021:3440427.

50 Paquette M, El-Houjeiri L, Pause A. mTOR pathways in cancer and autophagy. *Cancers (Basel)* 2018;**10**:. https://doi.org/10.3390/cancers10010018.

51 Li X, Yan J, Wang L, Xiao F, Yang Y, Guo X, *et al.* Beclin1 inhibition promotes autophagy and decreases gemcitabine-induced apoptosis in Miapaca2 pancreatic cancer cells. *Cancer Cell Int* 2013;**13**:1. https://doi.org/10.1186/1475-2867-13-26.

52 Oslowski CM. Stress responses: Methods and protocols. *Meas Autophagy Stress Cells* 2015:1–246. https://doi.org/10.1007/978-1-4939-2522-3.

53 Tyagi A, Gu M, Takahata T, Frederick B, Agarwal C, Siriwardana S, *et al.* Resveratrol selectively induces DNA damage, independent of Smad4 expression, in its efficacy against human head and neck squamous cell carcinoma. *Clin Cancer Res* 2011;**17**:5402–11. https://doi.org/10.1158/1078-0432.CCR-11-1072.

54 Alkhalaf M. Resveratrol-induced apoptosis is associated with activation of p53 and inhibition of protein translation in T47D human breast cancer cells. *Pharmacology* 2007;**80**:134–43. https://doi.org/10.1159/000103253.

55 Castellano-Pozo M, Santos-Pereira J, Rondón AG, Barroso S, Andújar E, Pérez-Alegre M, *et al.* R loops are linked to histone H3 S10 phosphorylation and chromatin condensation. *Mol Cell* 2013;**52**:583–90. https://doi.org/10.1016/j.molcel.2013.10.006.

56 Kao J, Salari K, Bocanegra M, Choi Y La, Girard L, Gandhi J, *et al.* Molecular profiling of breast cancer cell lines defines relevant tumor models and provides a resource for cancer gene discovery. *PLoS One* 2009;**4**:. https://doi.org/10.1371/journal.pone.0006146.

57 Tanner M, Kapanen AI, Junttila T, Raheem O, Grenman S, Elo J, *et al.* Characterization of a novel cell line established from a patient with Herceptin-resistant breast cancer. *Mol Cancer Ther* 2004;**3**:1585–92.

58 Szostakowska M, Trębińska-Stryjewska A, Grzybowska EA, Fabisiewicz A. Resistance to endocrine therapy in breast cancer: molecular mechanisms and future goals. *Breast Cancer Res Treat* 2019;**173**:489–97. https://doi.org/10.1007/s10549-018-5023-4.

59 Yanez M, Jhanji M, Murphy K, Gower RM, Sajish M, Jabbarzadeh E. Nicotinamide Augments the Anti-Inflammatory Properties of Resveratrol through PARP1 Activation. *Sci Rep* 2019;**9**:1–10. https://doi.org/10.1038/s41598-019-46678-8.

60 Cao X, Li C, Xiao S, Tang Y, Huang J, Zhao S, *et al.* Acetylation promotes TyrRS nuclear translocation to prevent oxidative damage. *Proc Natl Acad Sci U S A* 2017;**114**:687–92. https://doi.org/10.1073/pnas.1608488114.